Master's thesis

NTNU
Norwegian University of Science and Technology
Faculty of Information Technology and Electrical Engineering
Department of Electric Power Engineering

Bjørnar Hætta Turi

On-line Condition Assessment of 420 kV Terminations - design and development of partial discharge sensors

An experimental study on how transient magnetic fields affect an inductive partial discharge sensor

Master's thesis in Energy and the Environment
Supervisor: Frank Mauseth
Co-supervisor: Sverre Hvidsten and Hans Kristian Hygen Meyer
June 2023

NTNU
Norwegian University of
Science and Technology

Bjørnar Hætta Turi

On-line Condition Assessment of 420 kV Terminations - design and development of partial discharge sensors

An experimental study on how transient magnetic fields affect an inductive partial discharge sensor

Master's thesis in Energy and the Environment
Supervisor: Frank Mauseth
Co-supervisor: Sverre Hvidsten and Hans Kristian Hygen Meyer
June 2023

Norwegian University of Science and Technology
Faculty of Information Technology and Electrical Engineering
Department of Electric Power Engineering

NTNU
Norwegian University of
Science and Technology

Preface

This thesis is the final work of the 2-year master's program Energy and the Environment at the Norwegian University of Science and Technology (NTNU) under the Department of Electric Energy. The master's thesis accounts for 30 ECTS.

This master thesis is written as a part of the Smart on-line health Assessment of Cable Terminations (SmartACT) project, which is an ongoing innovation project between Statnett, Nexans, SINTEF and NTNU. This thesis is a continuation from the specialisation project completed in the autumn of 2022 and investigates how an inductive partial discharge sensor through the use of a High-Frequency Current Transformer (HFCT) will be affected by transient magnetic fields.

I would like to express my sincere gratitude to my supervisor, Associate Professor Frank Mauseth at NTNU, for his invaluable guidance, encouragement, and support throughout the course of this project. I would also like to thank both my co-supervisors from SINTEF, Research Scientist Hans Kristian Hygen Meyer, for his expert advice and contributions to this work and Senior Research Scientist Sverre Hvidsten, for his creative ideas.

In addition, I would like to acknowledge PhD candidate Paul Monceyron Røren for his guidance in the high current laboratory and all the people from the electrical workshop and service lab for their help with constructing parts and lending equipment related to the experiments.

Trondheim, 11th June 2023

Bjørnar Hætta Turi

Abstract

A cable termination is an essential component when transitioning from a cable to another power apparatus. However, it has been shown that cable terminations are more vulnerable to failure than the cable itself, mainly because they consist of a more complex geometrical structure and are installed on-site. This thesis is part of the SmartACT project, which aims to develop various sensors to warn before something goes wrong with 420 kV cable terminations. One of these sensors will detect partial discharges (PD) which is usually a sign that something is about to go wrong.

This master thesis is a continuation of the specialisation project completed in the fall of 2022 and is based on evaluating the effect transient magnetic fields have on the inductive PD sensor. The inductive PD sensor consists of wrapped copper mesh and a High-Frequency Current Transformer (HFCT) to inductively couple the partial discharge signals. However, the combination of the HFCT ferromagnetic core and the sensor being positioned inside the cable termination housing makes it susceptible to magnetic fields. To evaluate how the inductive sensor was affected by transient magnetic fields three experimental studies were conducted: 50 Hz AC current, switching transients and lightning impulses. In addition, magnetic field simulations in COMSOL were conducted to validate the experimentally found results.

The results from the 50 Hz AC current experiments revealed that both the orientation of the HFCT and distance away from the cable were significant factors in HFCT performance. For HFCT orientation, it was discovered that orientation 1 was substantially less affected by the magnetic field compared to orientations 2 and 3. For the distance between HFCT and the cable, it was found that an increase in distance will decrease the HFCT output voltage inversely proportionally.

Based on the conducted switching transient and lighting impulse experiments, it was discovered that high HFCT output voltage amplitudes can occur for an HFCT positioned inside a cable termination housing. The problem with the high voltage amplitudes is not related to the HFCT itself, but rather to the sensitive partial discharge measuring system. As a result, considerations to sufficiently dampen the voltage spikes should be taken and a proper protection scheme against overvoltages should be implemented.

Magnetic field simulations were successfully carried out in COMSOL, with the intention of verifying the 50 Hz AC current experiment results. Individual 3D models had to be created in order to facilitate the different orientations. The results from the magnetic field simulations generally aligned with the experimental findings, but some deviations were observed. It is assumed that the deviations mainly originated due to inaccurate modelling of the HFCT in COMSOL, unknown material composition of the ferrite core and low degree of model meshing.

This thesis provides a foundation for determining the optimal orientation and distance of the inductive sensor when installing it within a full-sized 420 kV oil-filled termination. Based on the experimental and simulation findings, it is recommended to position the HFCT in orientation 1, perpendicular to the cable. Additionally, it is advised to place the sensor as far away from the cable as possible, taking into account limitations imposed by the cable termination itself. To ensure the longevity required from the sensor, further work should involve establishing an overvoltage protection scheme.

Sammendrag

En kabelterminering er en nødvendig komponent når man går fra en kabel til et annet apparat i kraftsystemet. Det har derimot vist seg at kabeltermineringer er mer utsatt for feil enn kabelen i seg selv, mest fordi den består av en mer kompleks geometrisk oppbygging og installeres ute i felt. Denne masteroppgaven er skrevet som en del av SmartACT-prosjektet, som har som mål å utvikle ulike sensorer som skal kunne advare før noe går galt med 420 kV kabeltermineringer. En av disse sensorene skal oppdage partielle utladninger (PD) som vanligvis er et tegn på at noe er i ferd med å gå galt.

Denne masteroppgaven er en videreføring av spesialiseringsprosjektet som ble fullført høsten 2022, og baserer seg på å vurdere hvordan transiente magnetiske felt påvirker den induktive PD sensoren. Den induktive PD sensoren består av surret kobbernetting og en høyfrekvent strømtransformator (HFCT) for å induktivt koble partielle utladningsstrømmer. Men, kombinasjonen av HFCT'en sin ferromagnetiske kjerne og at den skal plasseres inni kabeltermingeringshuset, gjør den mer sårbar til magnetiske felt. For å vurdere hvordan den induktive sensoren ble påvirket av transiente magnetiske felt så ble det gjennomført tre eksperimenter: 50 Hz AC-strøm, koblingstransienter og lynimpulser. I tillegg så ble det utført magnetfeltsimuleringer i COMSOL for å validere de eksperimentelle funnene.

Resultatene fra 50 Hz AC-strøm eksperimentet viste at både orienteringen til HFCT og avstanden fra kabelen var betydelige faktorer for hvor påvirket HFCT'en ble. For HFCT-orienteringen, så ble det oppdaget at orientering 1 var betydelig mindre påvirket av det magnetiske feltet sammenlignet med orientering 2 og 3. For avstanden mellom kabelen og HFCT'en, så viste det seg at HFCT'ens utgangsspenning avtok omvendt proporsjonalt med økende avstand.

Resultatene fra eksperimentene med koblingstransienter og lynimpulser viste at det kan oppstå raske utgangsspenninger med høy amplitude for en HFCT som er plassert inn i termineringshuset. Problemet med de høye spenningsamplitudene er ikke relatert direkte til HFCT'en i seg selv, men heller til det følsomme systemet for deteksjon av PD. Derfor bør det tas hensyn til disse spenningsamplitudene, og som et resultat bør det implementeres en beskyttelsesordning mot overspenninger.

For å verifisere resultatene fra 50 Hz AC eksperimentet, ble det utført magnetfeltsimuleringer i COMSOL. Individuelle 3D-modeller ble laget for å legge til rette for de forskjellige orienteringene. Resultatene fra magnetfelt-simuleringene stemte generelt overens med de eksperimentelle funnene, men noen avvik ble observert. Det antas at avvikene hovedsakelig skyldes unøyaktig modellering av HFCT i COMSOL, ukjent materialoppbygning av kjerne og lav grad av masking i modell (meshing).

Denne oppgaven gir et grunnlag for å bestemme den optimale orienteringen og avstanden til den induktive sensoren ved installasjon i en fullskalert 420 kV oljefylt terminering. Basert på eksperimentelle og simuleringsfunn, anbefales det å plassere HFCT'en i orientering 1, vinkelrett på kabelen. I tillegg anbefales det å plassere sensoren så langt unna kabelen som mulig, med hensyn til begrensninger som finnes på innsiden i en kabelterminering. For å sikre den nødvendige levetiden til sensoren, bør videre arbeid innebære etablering av en beskyttelsesplan mot overspenning.

List of Symbols

ω	Angular frequency [rad/s]
σ	Electrical conductivity [S]
A	Magnetic vector potential [Tm]
B	Magnetic flux density [T]
C	Capacitance [pF]
D	Electric displacement field [C/m^2]
d	Thickness [m]
E	Electric field [kV/mm]
e	Induced voltage [V]
f	Frequency [Hz]
H	Magnetic field strength [A/m]
I	Current [A]
J	Current density [A/m^2]
L	Inductance [mH]
M_i	Mutual impedance [H]
M	Magnetisation of material [A/m]
R	Resistance [Ω]
r	Radius [mm]
U	Voltage [V]
x	Distance [mm]
y	Distance [mm]
Z	Impedance [Ω]
Z_m	Measuring impedance [Ω]
μ	Permeability [H/m]
μ_r	Relative permeability [H/m]
μ_0	Permeability of free space [H/m]

List of Abbreviations

AC	Alternating Current
AI	Artificial Intelligence
CAD	Computer Aided Design
CB	Circuit Breaker
CZ	Current Zero
DC	Direct Current
FEM	Finite Element Method
FFT	Fast Fourier Transformation
HV	High Voltage
HFCT	High-Frequency Current Transformer
IEC	International Electrotechnical Commission
LCD	Liquid Crystal Display
OHL	Overhead Line
PD	Partial Discharge
PEX	Cross-linked Polyethylene
RF	Radio Frequency
RMS	Root Mean Square
SC	Short Circuit
SW	Switch Breaker
TOV	Transient Overvoltages
TRV	Transient Recovery Voltage
TSO	Transmission System Operator

Table of Contents

List of Figures

List of Tables

1 Introduction

Norway's transmission grid is made up of overhead lines and cables with voltages up to 420 kV. Although overhead lines make up the majority of the transmission grid, in particular locations, such as fjord crossings and densely populated areas, cables may be the only option. When transitioning from a cable to another component, it will be essential to use an end termination, also known as a cable termination, that is engineered to withstand the service stresses that are expected [1]. At the highest voltage level in the Norwegian transmission grid, these cable terminations are usually oil-filled. Figure 1.1 illustrates such an oil-filled cable termination for polymer cables with a voltage rating of up to 550 kV.

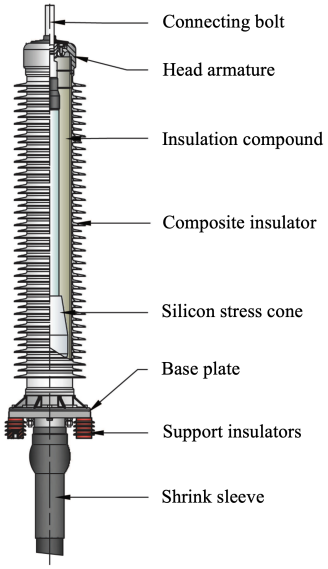

Figure 1.1: Oil-filled outdoor cable termination for polymer cables rated up to 550 kV [2].

Cable accessories, such as joints and terminations, are more likely to cause operational disturbances than the cable itself, due to the strict manufacturing processes and test procedures the cable undergoes. There are several factors that contribute to cable terminations being more vulnerable to faults. Firstly, a cable termination consists of a complex structure with field grading material and sometimes several dielectrics. Secondly, they are done on-site which increases the risk significantly for defects and contaminants. Contaminants, such as particles, dust, or moisture are the biggest threats when installing terminations on site [3], [4].

Despite the fact that cable terminations are more vulnerable to electrical breakdown, they rarely fail in Norway. According to Statnett, the Norwegian TSO, there have only been ten incidents involving 420 kV cables that have caused operational disruption from 2009 to 2022. Only one of these ten incidents can be directly linked to cable accessories such as a cable termination [5]. However, a cable termination is a critical component in the power system and a breakdown will have many negative consequences, such as power outages and high non-delivered energy costs [4].

Previous research has revealed that the most typical reason of a cable termination breakdown is due to the slow and gradual degradation of the insulating material caused by partial discharges (PD). Therefore, measurement of PD activity is an attractive option for condition assessment of terminations, especially on-line measurements. On-line PD measurement allows for continuous monitoring of the power apparatus condition without disrupting the electrical service [6].

The commonly used method for PD detection, the conventional method, is only possible for off-line measurements. As a result, in order to obtain on-line measurements, non-conventional techniques such as inductive coupling has to be used. Inductive coupling of PD current is done through the use of a High-Frequency Current Transformer (HFCT), which is an attractive option as it can detect even the smallest PD amplitudes, and thus offers a high sensitivity [7].

1.1 Condition assessment

Condition assessment can be explained as the comparison between the current condition state and another reference condition state. Based upon the comparison, appropriate condition rating schemes should decide whether measures should be taken [8]. Figure 1.2 shows how the condition assessment of a component can be done in order to establish its technical condition.

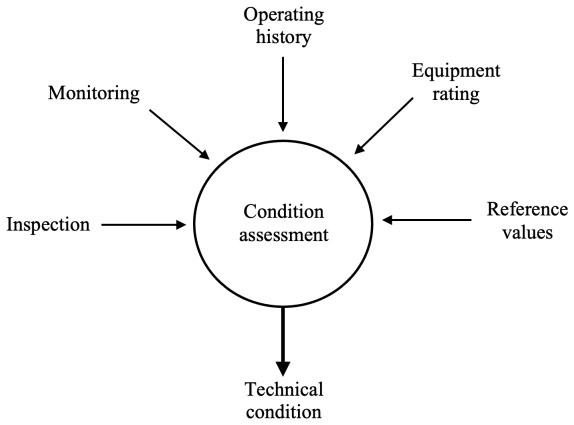

Figure 1.2: A general layout of the condition assessment for a component. The inputs to the condition assessment are the ratings of the equipment, operation history, reference values and indicators from inspection and monitoring [8].

Condition assessment of a component in the power system is the evaluation of what can go wrong, how it can be measured, and how the measured results can be interpreted. A power system consists of power apparatuses for generation and transmission which are technically advanced. However, they are made from an economic perspective to maintain a reliable power supply at as low of a cost as possible, thus making them more vulnerable to faults and ageing [9].

It is common to differ between two types of diagnostic methods in the power system: on-line and off-line. On-line condition assessment involves diagnostic techniques while the object or component is in normal operation, while off-line condition assessment requires the apparatus to be taken out of service. On-line diagnostic methods are preferable and ideally, they should also be non-destructive, related to a known failure, easy to operate and less expensive than a replacement of component [10].

1.2 SmartACT

SmartACT, Smart On-Line Health Assessment of Cable Terminations, is an innovation project that aims to develop a measurement system based on several sensors inside 420 kV cable terminations. The project is a collaboration between Statnett, Nexans, Sintef and NTNU, and is financed by The Research Council of Norway [11].

The purpose of a measurement system like this is to provide an early warning when something is about to go wrong. The sensor signals must be wirelessly transmitted, and the electronics must be powered wirelessly. Processing of the data shall be done with Artificial Intelligence (AI). Due to the long lifetime of the cable termination, it is necessary to have an equally long, or longer, lifetime for the sensor [12].

Statnett, the Norwegian TSO, has experienced that delivered cable terminations do not include any type of monitoring system and are considered maintenance-free. However, the consequences of a failure will result in negative economic consequences such as loss of high not-delivered costs. If the project is to succeed, it can provide major savings, more efficient operation, and maintenance, as well as fewer accidents [13].

1.3 Scope of thesis

This master's thesis builds upon the specialization project that was completed in the fall of 2022 [14]. The earlier study investigated two sensor proposals, capacitive and inductive coupling, evaluating their positioning and sensitivity as crucial evaluation criteria. The results demonstrated that the capacitive sensor performed better, exhibiting a higher and more stable sensitivity than the inductive sensor.

The PD sensor will be installed within the termination housing, and it was discovered that the use of the capacitive sensor would require minor modifications to the 420 kV termination housing, leading to the necessity for a new type approval of the entire termination. As a result, it has been decided that the inductive partial discharge sensor will be used and consequently will be the focus throughout this thesis.

The inductive partial discharge sensor is constructed of copper mesh surrounding the stress cone and cable with the use of a High-Frequency Current Transformer (HFCT) to inductively couple the signals. However, the combination of the HFCT ferromagnetic core and the sensor being positioned inside the cable termination housing makes it susceptible to magnetic fields. This laid the foundation to evaluate the effect that transient magnetic fields have on the inductive partial discharge sensor. To achieve this, a combination of experimental work and magnetic field simulations in COMSOL were conducted.

To begin with, high current experiments at the network frequency of 50 Hz were conducted to establish a baseline on how the magnetic field emitted from a cable would affect the inductive PD sensor. As mentioned, the HFCT becomes susceptible to nearby magnetic fields, however, the orientation of the HFCT was suspected to have a big influence on how greatly it was affected. As a result, three different HFCT orientations were tested and in addition, the distance between the HFCT and cable was varied.

Following the 50 Hz AC current experiments, switching transient experiments were conducted in an attempt to artificially create a fast-acting transient current that occurs during a re-strike. The final experiment was done with lightning impulses which have the ability to create a very-fast transient current and resulting magnetic field. Lastly, magnetic field simulations were conducted in COMSOL with the purpose of validating the results obtained from the 50 Hz AC current experiments.

To summarize, this thesis will investigate the following:

- Experiments with 50 Hz AC current - Measurement of magnetic flux density, analysis of voltage waveform and magnitude for three HFCT orientations and at different distances from the cable.
- Experiments with switching transients - Measurement of HFCT output voltage during short circuit current, current interruption and current re-strike.
- Experiments with lightning impulses - Measurement of HFCT output voltage during very fast-acting transient current.
- Magnetic field simulations in COMSOL - Simulations of magnetic flux density from a cable and HFCT output voltage at different orientations and distances.

1.4 Structure

This thesis is structured into 7 sections, starting with this introduction where the background, project description and scope of the thesis have been presented.

In Section 2, the relevant theory to understand how an inductive partial discharge sensor works and how electrical transient magnetic fields may influence it is covered.

In Section 3, the methodology for the experimental work conducted will be thoroughly described. Each experiment will follow the same structure, starting by presenting the experimental setup before specifying the tests performed.

In Section 4, the obtained results will be presented as plots and figures where the most important findings will be briefly discussed. The presented results follow the same structure as Section 3.

In Section 5, comparison and evaluation of all the gathered results will be done in the form of plots and figures. Following the comparisons, further discussions about possible faults and errors encountered will be mentioned.

In Section 6, a conclusion will be drawn based on the most important experimental findings throughout the thesis.

In Section 7, suggestions to further work will be given based on this thesis's findings.

Lastly, some important remarks about this thesis will be mentioned.

- It is assumed that the reader is familiar with basic electrical engineering.
- Several parts from the specialization project [14] completed in the fall of 2022 has been reused in the Section 1 & 2.

2 Theory

This section will present the theoretical knowledge necessary to understand how an inductive partial discharge sensor can be affected by transient magnetic fields within a high voltage cable termination. Firstly, a background in the purpose and technology of cable terminations will be presented. Secondly, theory on partial discharges will be presented before explaining how the inductive partial discharge works. Then, electrical transients that may occur in cable systems and necessary background theory on magnetostatics will be presented. Lastly, the section concludes with a presentation of the theoretical background knowledge necessary for understanding how magnetic field simulations are performed in COMSOL.

2.1 Cable termination purpose and technology

A cable termination is a necessary component when connecting a cable to another apparatus or part of the installation due to the geometrical changes that take place. The geometrical changes involve exposing the conductor in order to ensure proper electrical connection between the cable and another electrical apparatus. This implies that the cable insulation has to be peeled and the outer screen also has to be removed a bit further back from the insulation [1].

The main problem when exposing the bare insulation is the high electric field present at the separations between the outer semi-conductor and the bare insulation, as shown in Figure 2.1. In air, this high electric field may cause partial discharges along the surface. If the voltage is to be increased, then the discharges may eventually flash over to the conductor [15].

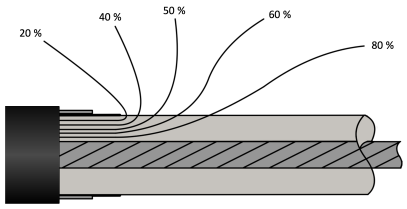

Figure 2.1: Illustration of the equipotential lines for a cable termination with no field control modifications. The high electric field in the separations between the outer semi-conductor and insulation may cause surface discharges.

As a result, it is necessary to control the field strength caused by geometrical changes in the cable structure. There are many techniques to accomplish this, however a prefabricated stress cone is frequently used for a high voltage oil-filled cable termination. Figure 2.2 shows such a stress cone and how the corresponding field changes.

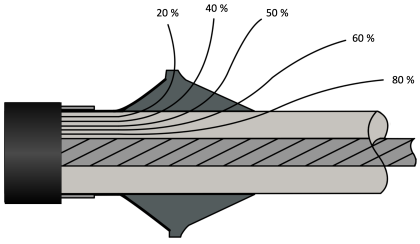

Figure 2.2: Illustration of the equipotential lines for a cable termination with a stress cone. The electric field is spread out evenly so that no unwanted discharges occur.

The stress cone is engineered to spread out the field, reducing the field strength to an acceptable level in both the solid insulation and the surrounding air or other insulating mediums.

At higher voltage levels, the stress cone is usually made of either ethylene-propylene elastomer (EPR) or silicone rubber and is positioned inside the cable termination housing [16]. Figure 2.3 illustrates an outdoor composite cable termination with the dimensions for 420 kV polymeric cables with a stress cone fitted.

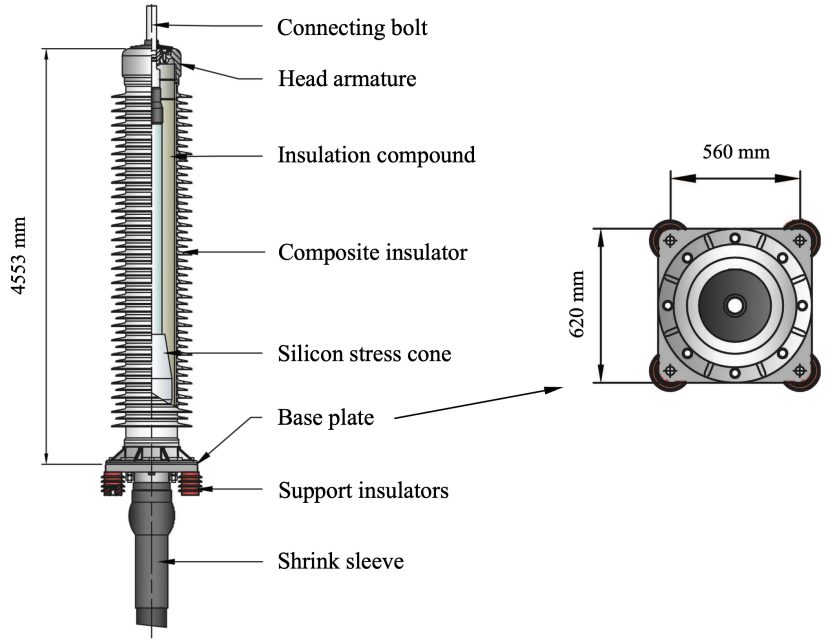

Figure 2.3: Illustration of a composite outdoor cable termination with dimension for 420 kV polymeric cables. The insulating compound consists of a highly insulating material, which for this type of outdoor cable termination is silicone oil [2].

A high voltage termination is usually positioned outdoors but inside a substation where every square meter is expensive. This reflects on the dimensions of cable termination with its significant height of 4.55 meters, but its width is comparatively narrow with a base plate dimension of only 620x620 mm. This poses some limitations when installing the inductive partial discharge sensor inside the termination housing.

Because the inductive partial discharge sensor will be installed inside the cable termination enclosure, the inside dimension becomes critical. The inner diameter of the termination housing is estimated to be 500 mm based on the base plate specifications provided in Figure 2.3. Considering a PEX insulated cable with a conductor cross-section of 2500 mm^2, it will have a diameter of roughly 190 mm. As a result, the distance between the outer semi-conductor of the cable and the inner termination housing wall will be small, in this case only 155 mm.

2.2 Partial discharge

Partial discharge (PD) is a common denominator for phenomenons where a discharge will short circuit a part of the insulation, and is according to IEC 60270 [17] defined as:

> *"A localized electrical discharge that only partially bridges the insulation between conductors and which can or can not occur adjacent to a conductor"* [17].

In order for a partial discharge to occur, then two conditions have to be met. Firstly, the electric field has to be high enough to initiate a local electron avalanche. Secondly, the local electric field must be higher than the local withstand ability [18].

An insulation material that is dielectrically stressed can be compared to a capacitor, as there will be stored potential electric field energy. Upon a discharge in the insulation, this energy will be released and a transformation to other energy forms will take place. The energy will be transformed into a number of other forms, as shown in Figure 2.4 [18].

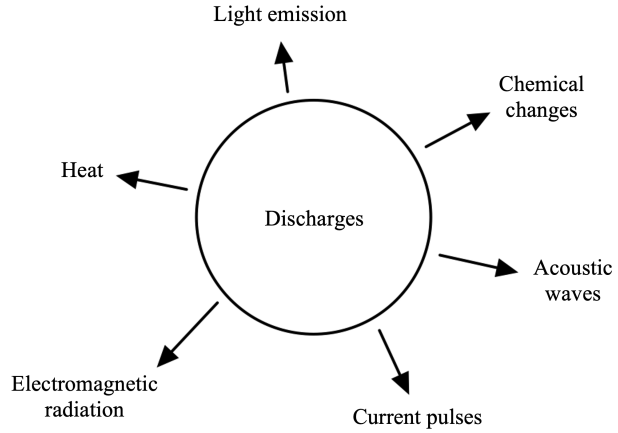

Figure 2.4: Locally stored energy in insulation that will be transformed to other forms of energy. The energy transformations cause degradation of solid insulation materials; however, it serves as the foundation for PD measurements [18].

The resulting energy transformation is responsible for degradation of some insulating materials, such as a cable with PEX insulation. The degradation of the insulation occurs due to three reasons: bombardment of ions and accelerated electrons, chemical reactions with a following temperature rise and radiation. However, some insulating materials, such as air, have self-healing properties following a discharge [15], [18].

But more importantly for this project, the energy transformation lays the foundation for PD measurement. The resulting acoustic waves, electromagnetic radiation and current pulses can be used to detect partial discharges [19].

2.2.1 Partial discharges in cable systems

There are two types of partial discharges that can occur in cable systems: internal and exterior discharges. External discharges are related to discharge on the exterior of the cable, such as surface and corona discharges. But in a cable system, internal discharges are the biggest threat to the cables insulation system [20].

As stated in the introduction, the cable will go through several tests before being released from the factory. As a result, the main concern is not the cable itself, but rather the cable accessories such as cable joints and terminations. This is primarily due to two factors. First, cable accessories have more complex structures that include field grading materials and multiple dielectrics. Second, it is installed on-site, which significantly increases the possibility of contaminants [3], [4].

Cable terminations have strict installation procedures and any deviation from these will pose a threat to the cable's integrity. Some typical mistakes done during the instalment are wrongly aligning the stress cone and having contaminants get under the stress cone. A wrongly aligned stress cone with respect to the outer semi-conductor can lead to the formation of voids [21]. Figure 2.5 illustrates these common mistakes and the possible consequence.

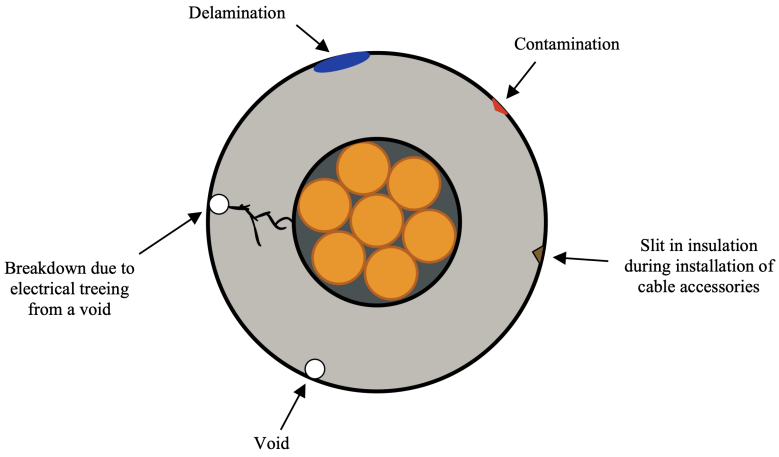

Figure 2.5: Types of common cable defects and possible consequences. The most common ones are void formation and contaminants.

Voids can be a result of improper installation of the stress cone. Contamination, especially of inductive impurities, occurs due to a low degree of cleanliness during installation. Slits or cuts in the cable insulation occur due to improper training and rough handling during installation.

Commonly for all the mentioned is that they can cause degradation of the solid insulation due to partial discharges. If the degradation due to partial discharges remains unnoticed, then the voids, contaminations and slits can progress into electrical treeing and potentially a complete breakdown of the cable system [15], [22].

2.3 Inductive partial discharge sensor

Inductive sensors, or couplers, can be used to measure the magnetic part of the electromagnetic field emitted by a partial discharge. This is achieved by using a High-Frequency Current Transformer (HFCT) which is made up of an induction coil with a ferromagnetic core. There are several types of HFCTs available on the market, where the main difference is how large the primary current can be and the frequency bandwidth they offer. Figure 2.6 presents the working principle of an inductive sensor when current from partial discharges travels through the ground conductor.

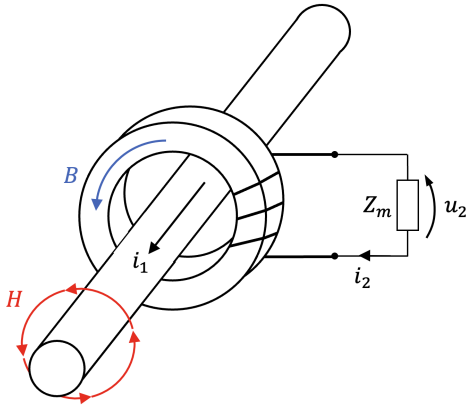

Figure 2.6: The working principle of an HFCT; A current caused by partial discharges in the ground connector will generate a magnetic field H and a corresponding magnetic flux B in the HFCT core. This magnetic flux will generate a voltage u_2 in the secondary winding [7].

The ground conductor will act like a one-turn winding on the primary side and the secondary side is short-circuited with a low-ohmic resistance. During partial discharges, the ground conductor will have induced small high-frequency currents from the partial discharges which are detectable by the use of a HFCT. The high-frequency currents will excite a magnetic field, H, which will be concentrated as magnetic flux in the HFCT core, which in turn will generate a voltage in the secondary winding [7], [23].

An inductive sensor through the use of a High-Frequency Current Transformer aligns well with the current characteristics produced by partial discharges, usually lasting in the range of nanoseconds resulting in frequencies in the MHz range [19]. The sensor follows Faraday's law, and the resulting transfer function is shown in Equation 2.1. The transfer function explains that the induced voltage, e, is proportional to the change rate of the current times the constant mutual impedance $\mathbf{M}_i$ between the primary and secondary side [24].

$$\mathrm{e} = \mathbf{M}_i \frac{di}{dt} \tag{2.1}$$

As previously stated, there are numerous variants of HFCTs on the market, with the key difference being that they offer different frequency bandwidths and maximum tolerated primary current. The frequency bandwidth of HFCTs can range from 0.5 Hz to 1 GHz and is mostly determined by three key factors: the ferrite core's material composition, the number of turns, and the size of the air gap within the core.

Soft magnetic ferrite cores are commonly used for current transformers that require a high-frequency bandwidth, such as an HFCT. Examples of typically used ferrite cores for HFCT are Nickel-Zinc (NiZn) and Mangenese-Zinc (MnZn). NiZn is normally used when the demand for frequency bandwidth is over 3 MHz, while MnZn ferrite cores normally are used for frequency bandwidths below 3 MHz [7].

Earlier studies [7], [25] and [26] show that the number of secondary winding turns poses a great influence over the sensitivity and frequency bandwidth. Fewer turns give a better sensitivity, which is desirable, but will however increase the lower frequency bandwidth cut-off. As a result, the HFCT may not be able to properly detect partial discharge signals in the lower end of the frequency bandwidth. Therefore, the number of turns should be carefully considered based on the sensor's application.

The presence of air gaps within the ferrite core of a High-Frequency Current Transformer will lead to a reduction in sensitivity across its entire frequency bandwidth. Thus, to achieve maximum sensitivity it is recommended to use closed toroidal ferrite cores. The closed toroidal core can either be in one piece or through a split core for easier installation. However, if there are concerns for core saturation then air gaps can be implemented which will in turn reduce the possibility of saturation. The size of the ferrite core imposes only a small influence on the frequency bandwidth, where a large core size will increase the cut-off frequency bandwidth slightly compared to a smaller core of the same material [7], [27].

The use of an inductive sensor for partial discharge measurements is an attractive alternative due to the non-intrusive installation it offers. The inductive sensor is already a well-established PD detection method for power transformers, and the same principles can be used for cable terminations, with some slight modifications. The modification needed is some conducting material, such as copper mesh or foil, preferably located directly over the expected PD location to provide a capacitive coupling to the defect [6].

HFCT sensitivity is how well the primary current is inductively coupled and transformed to the secondary side and can be calculated as the transfer impedance given through Equation 2.2. The transfer impedance will be frequency dependent, due to the frequency dependency of the ferrite core [27].

$$Z_T = \frac{u_2}{i_2} \tag{2.2}$$

As previously mentioned, an HFCT is ideal to detect partial discharges due to the high-frequency bandwidth it offers. However, it can also be a problem when it is exposed to fast-acting electrical transients, which will be covered in the next subsection.

2.4 Electrical transients in cable systems

Electrical transients that occur in cable systems are different from the ones that occur in overhead lines (OHLs). Electrical transients in OHLs are commonly referred to as lightning events and are tested according to lightning impulse procedures. Conversely, electrical transients in cables are primarily caused by the closing and opening of circuit breakers and switches. However, cables may also be subjected to lightning impulses in instances where overhead lines transition to an underground cable prior to reaching the substation [28].

This subsection will cover the relevant overvoltages and overcurrents that can occur to a cable and its accessories, and how they can be tested according to international standards. To begin with, lightning impulses will be described before moving on to switching overvoltages, where the focus will be on circuit breaker re-strike.

2.4.1 Lightning impulses

Lightning overvoltages originate as the name states from lightnings, and will as previously mentioned only affect the cable systems if an overhead line transitions to a cable without proper surge arresters. Lightning overvoltages is a very fast-acting voltage, usually in the range of microseconds.

When producing lightning impulses, current amplitudes in the range of hundreds and voltage in the range of thousands are required. A commonly used circuit for impulse voltage testing is through the use of a Marx generator. A Marx generator consists of charged capacitors that can transfer its stored energy into the test object upon triggering spark gaps. The Marx impulse generator can be stacked in stages, which will increase the transferred energy and the voltage multiplication accordingly [29].

According to IEC 62067 [30], the voltage for the lightning impulse test shall be 1425 kV for a 420 kV cable. The shape of the test shall be a standard 1.2/50 lighting impulse, implying that the front time, T_1, is 1.2 μs with a half-value time, T_2, of 50 μs. Some tolerances are made allowing for 1.2 $\pm$ 0.36 μs for the front time and 50 $\pm$ 10 μs in half-value time.

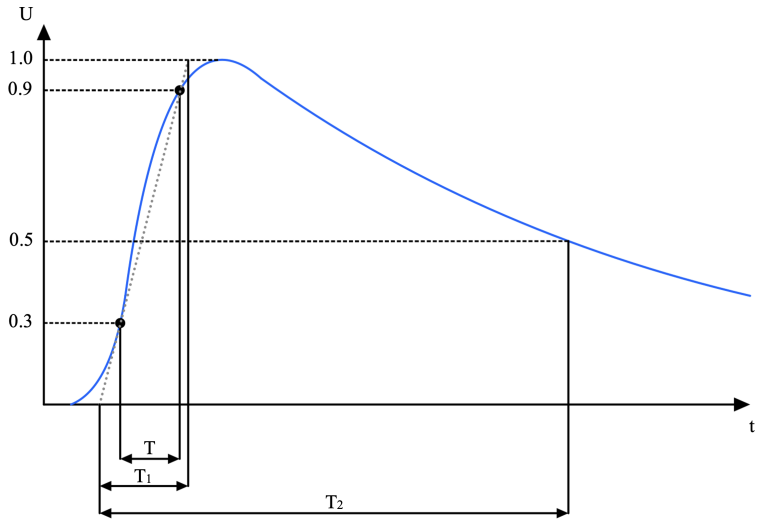

Figure 2.7: Standard lightning impulse voltage with the relevant time parameters T_1, T_2 [31].

However, it is not the voltage that is responsible for generating the magnetic field. The resulting current from a lightning impulse will be an exponential impulse current, as presented in Figure 2.8.

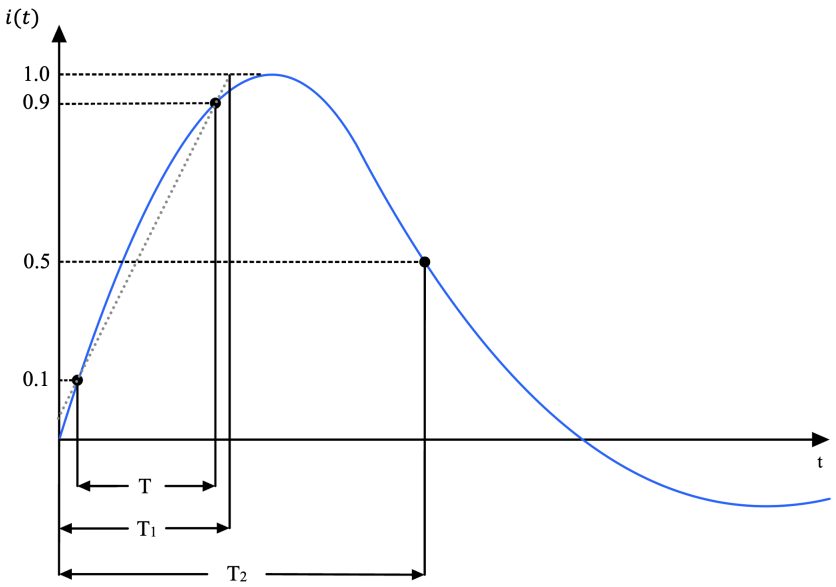

Figure 2.8: Exponential impulse current with the relevant time parameters T_1, T_2 [23].

Typically, the decrease of the impulse occurs as a heavily damped sine wave or exponentially. A heavily damped sine wave is expected to drop below zero, causing a polarity reversal as present in Figure 2.8 [23].

2.4.2 Switching overvoltages

Switching overvoltages are phenomenons that occur during circuit breaker and switching operations in the power grid. A switching overvoltage is also characterized as a fast-acting transient, however, it is slower than the previously explained lighting impulse. The amplitude of the voltage is determined upon when the circuit breaker or switch is initiated in relation to the source voltage waveform.

Cables, which can be considered as a capacitive load, undergo the worst scenario if an attempted current interruption turns into a re-strike. A potential re-strike comes as a result of earlier energizing of the capacitive load, where the inrush current with a following pre-arc will result in degradation of the breaker contact surfaces. Once the contact surfaces are degraded, then the transient recovery voltage (TRV) becomes a critical factor and may cause re-strikes [32]. Figure 2.9 presents a circuit diagram representing a capacitive load being interrupted. The stray capacitances on the load side are much greater than the stray capacitances on the source side, $C_2 \gg C_1$.

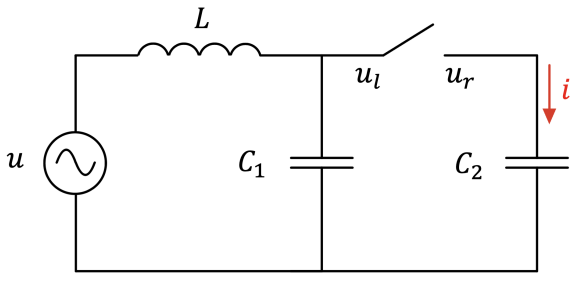

Figure 2.9: Circuit diagram of a capacitive load that is to be interrupted, where $C_2 \gg C_1$ [32].

If the re-strike should occur when the recovery voltage reaches its maximum, then the result on the load side is a fast oscillating voltage. Also, the magnitude of the load side voltage will be nearly 3 times the

source voltage [33]. Figure 2.10 presents a capacitive current interruption followed by a re-strike and another current interruption.

Figure 2.10 presents the current and voltages during a capacitive current interruption followed by a re-strike and another current interruption. Initially, the current is interrupted at the first current zero (CZ) crossing, before a re-strike occurs when the recovery voltage u_r is at its maximum.

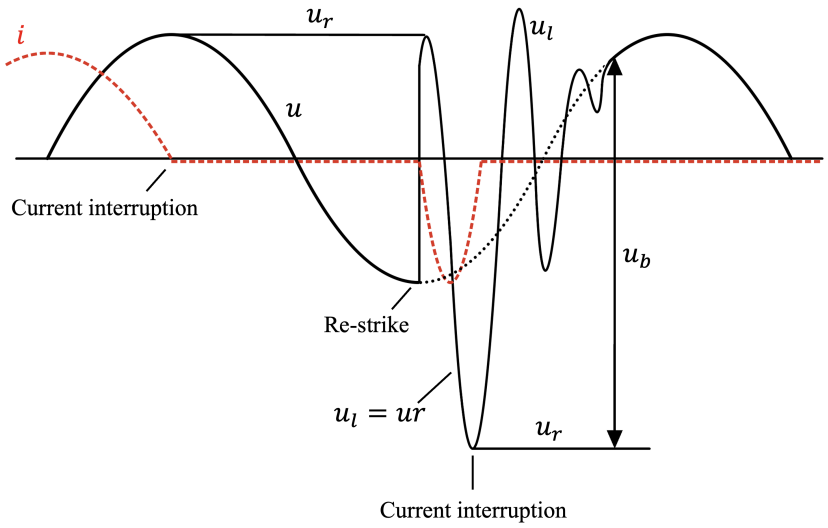

Figure 2.10: Current and voltage waveforms during a current interruption, restrike and a following current interruption. The voltage will experience oscillation during the re-strike [32].

The result of a re-strike at the maximum TRV is a fast oscillating voltage, where the voltage magnitude on the load side will be nearly 3 times the source voltage. But more importantly for the generation of transient magnetic fields, it will cause a fast-acting transient current.

In order to accommodate these fast-acting transients, international standards, such as IEC 62067 [30] recommend performing switching impulse tests. The standard switching impulse is defined as a 250/2500 impulse test, implying a peak time, T_p, of 250 μs and a 2500 μs half-time value, T_2.

2.5 Magnetostatics

Magnetostatics is a discipline in electromagnetism which describes the static magnetic field, generated by either a permanent magnet or a steady electric current. Even though it only applies to static magnetic fields, it lays the foundation for magnetic fields produced by alternating currents (AC). This subsection will begin by explaining some basic magnetic field theory before progressing to the magnetic field emitted from an AC power cable. Lastly, it will define magnetic materials and how magnetic saturation can occur for a ferromagnetic material.

2.5.1 Magnetic field

Magnetic fields are produced as a result of electric current and magnetized materials. Especially electricity and magnetism are closely connected and the relationship between them can be seen through Maxwell equations. To explain the magnetic field, both the **B**-field and **H**-field are used. The alternative name for **B**-field is magnetic flux density and for **H**-field it is magnetic field strength. Maxwell's equation in Equation 2.3 reveals that the magnetic flux density is divergenceless, implying that the flux in a closed surface is zero [34].

$$\nabla \cdot \mathbf{B} = 0 \tag{2.3}$$

For a steady current density **J**, the magnetic flux density can be calculated through Equation 2.4.

$$\nabla \cdot \mathbf{B} = \mu_0 \mathbf{J} \tag{2.4}$$

which, as presented in Equation 2.5, becomes Ampére's law when expressed in integral form.

$$\oint_S \mathbf{B}\, dS = \mu_0 I \tag{2.5}$$

Where, μ_0 is the permeability of free space, I is the current and S is the closed surface. Next, the magnetic field strength **H** is an auxiliary field that occurs when dealing with magnetic materials. In free space, the relationship between magnetic field strength **H** and magnetic flux density **B** is only related through the permeability of free space μ_0, as shown in Equation 2.6.

$$\mathbf{B} = \mu_0 \mathbf{H} \tag{2.6}$$

Combining $\mathbf{B} = \mu_0 \mathbf{H}$ and $\nabla \times \mathbf{B} = \mu_0 \mathbf{J}$, the magnetic field strength given a steady current density **J** is shown in Equation 2.7.

$$\nabla \cdot \mathbf{H} = \mathbf{J} \tag{2.7}$$

If expressed in integral form it becomes the Ampére's law for magnetic field strength, as presented in Equation 2.8.

$$\oint_c \mathbf{H}\, dl = I \tag{2.8}$$

2.5.2 Magnetic field from cable

Whenever an electric current is flowing through a conductor there will be a magnetic field produced around it. For a conductor carrying a constant current, the magnetic flux density at any given point in space can be calculated through Biot-Savarts Law presented in Equation 2.9 [34].

$$\mathbf{B}(x, y, z) = \frac{\mu_0}{4\pi} \oint_C \frac{Idl \times \hat{\mathbf{r}}}{r^2} \tag{2.9}$$

Where **B** is the magnetic flux density, μ_0 is the permeability of free space, I is the current flowing through the conductor, dl is a small length of the conductor and r is the distance from dl to the given point.

However, under the assumption that the conductor has a cylindrical shape, is infinitely long and one dimension can be ignored, an easier approach can be used through Ampere's Law. Equation 2.10 presents the Ampere's law for magnetic flux density **B**, where μ_0 is the permeability of free space, dS is the closed magnetic flux surface, and I is the current flowing through the conductor [35].

$$\oint_S \mathbf{B}\, dS = \mu_0\, I \tag{2.10}$$

For a coaxial wire configuration, the integral in Ampere's law corresponds to the circumference of $2\pi r$. As a result, the magnetic flux density **B** at a radial distance of r from the cable is given by Equation 2.11.

$$\mathbf{B} = \frac{\mu_0\, I}{2\pi r} \tag{2.11}$$

Given a constant current, the magnetic flux from the cable will decrease inversely proportionally at a rate of $\frac{1}{r}$. This is illustrated in Figure 2.11, which also shows the magnetic field direction given that the current direction is towards the reader. The magnetic field direction can also be described through the right-hand rule, where the thumb indicates the current carrying conductor and the wrapped fingers indicate the magnetic field direction.

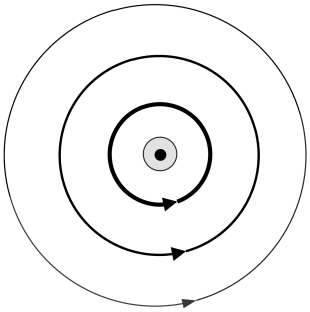

Figure 2.11: Illustration of the magnetic field direction and magnitude from an infinitely long wire, where the current direction is coming towards the reader.

2.5.3 Magnetic materials

Magnetic materials can be separated into the following three categories: diamagnetic, paramagnetic and ferromagnetic materials. A diamagnetic material has a relative permeability lower than 1, while a paramagnetic material has a relative permeability higher than 1. Both diamagnetic and paramagnetic materials share the characteristic of having a linear relative permeability with respect to magnetic field frequency, with a value of ~ 1.

Ferromagnetic materials, on the other hand, behave non-linearly and are affected by the frequency, magnitude and history of the applied magnetic field. However, it is common to define a relative permeability based on the average slope number of the hysteresis curve B(H). Table 2.1 presents some examples from the three mentioned magnetic material categories [35].

Table 2.1: Relative permeability of some diamagnetic, paramagnetic and ferromagnetic materials under room temperature. Ferromagnetic materials are non-linear, therefore the permeability is the average slope number for the hysteresis curve [35].

Diamagnetic		Paramagnetic		Ferromagnetic	
Material	$\boldsymbol{\mu_r}$	**Material**	$\boldsymbol{\mu_r}$	**Material**	$\boldsymbol{\mu_r}$
Gold	0.99996	Air	1.0000004	Iron + 4% silicon	7000
Copper	0.999991	Aluminium	1.00002	Pure iron	$2 \cdot 10^5$
Wood	0.9999995	Platinum	1.00026	Supermalloy	$\sim 10^6$

The permeability of a ferromagnetic material is dependent on the frequency of the magnetic field it is exciting, as shown in Equation 2.12 [7].

$$\mu(f) = \mu'(f) - j\mu''(f) \tag{2.12}$$

Where μ' refers to the relative material permeability and the imaginary part μ'' refers to the hysteresis losses.

2.5.4 Magnetic saturation

Magnetic saturation is a problematic scenario for all types of transformers as the core is made up of ferromagnetic material. Saturation of ferromagnetic materials occurs when the applied magnetic field strength reaches a high enough level, causing the magnetic molecules within the material to align themselves to the field. Once the molecules are aligned to the magnetic field, then the magnetic flux density from the molecules in the material will not contribute anymore, and thus the relationship between magnetic field strength and magnetic flux density will increase non-linearly.

Figure 2.12 presents the relationship between the magnetic field strength **H** and magnetic flux density **B** when a ferromagnetic material goes into saturation [36].

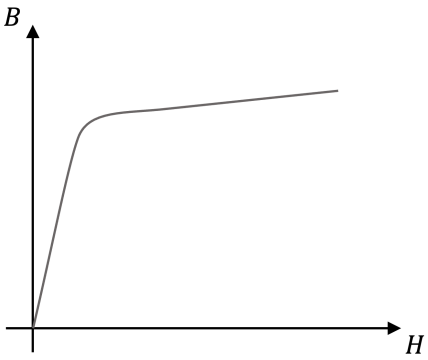

Figure 2.12: Magnetic saturation of an magnetic material. When the magnetic field strength H is increased over a certain level, then the magnetic flux density B will not increase linearly [36].

Once a transformer reaches saturation, disproportional high levels of magnetic field force are required to deliver the demand in magnetic field flux. This causes the induced voltage and current in the secondary winding to become distorted due to harmonics. Typical output voltage of a saturated current transformer can be seen in Figure 2.13, where i_1 is the input current and u_2 is the output voltage [27].

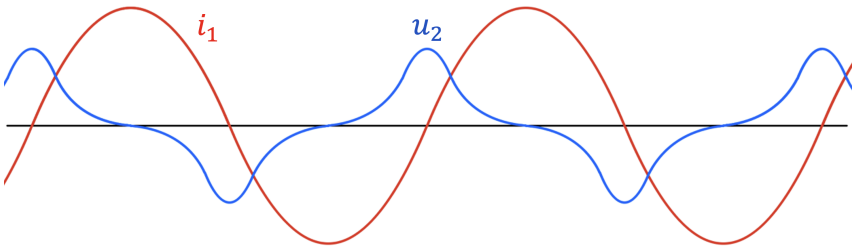

Figure 2.13: Illustrative example of a current transformer experiencing core saturation, where i_1 is the input current and u_2 is the output voltage. The core saturation causes the output voltage u_2 to become distorted.

For a High-Frequency Current Transformer, the biggest threat to core saturation comes from the high magnetic field at the power frequency of 50 Hz. A potential 50 Hz core saturation of the HFCT will reduce its sensitivity to detect partial discharges over its entire frequency bandwidth. Thus, measures to prevent core saturation when using an HFCT for partial discharge detection should be of high priority. These measures can be magnetic field shielding or implementation of an air gap in the core [7], [37].

2.6 Magnetic Field Simulation

COMSOL Multiphysics provides a diverse range of simulation models based on Finite Element Method (FEM). For investigating the magnetic field generated by a current at the network frequency, the most suitable option is the AC/DC model with the Magnetic Fields interface. The equation that solves the induced current and magnetic fields in the frequency domain is derived from Ampère's Law, which includes displacement currents. The equation is as follows:

$$\nabla \times \mathbf{H} = \mathbf{J} + \frac{\partial \mathbf{D}}{\partial t} = \sigma \mathbf{v} \times \mathbf{B} + \mathbf{J}_e + \frac{\partial \mathbf{D}}{\partial t} \tag{2.13}$$

Where, $\mathbf{H}$ represents the magnetic field strength, $\mathbf{J}$ is the current density, $\mathbf{D}$ is the electric displacement, σ denotes electrical conductivity, $\mathbf{v}$ denotes the conductor's velocity, $\mathbf{B}$ is the magnetic flux density and $\mathbf{J}_e$ is the current density generated externally.

Assuming a time-harmonic field, $\mathbf{B}$ and $\mathbf{E}$ can be defined as:

$$\begin{aligned} \mathbf{B} &= \nabla \times \mathbf{A} \\ \mathbf{E} &= -j\omega \mathbf{A} \end{aligned} \tag{2.14}$$

Here, $\mathbf{E}$ is the electric field vector and $\mathbf{A}$ is the magnetic vector potential. By incorporating these definitions into Ampère's Law and utilizing the relationships $\mathbf{B} = \mu_0(\mathbf{H} + \mathbf{M})$ and $\mathbf{D} = \varepsilon_0 \mathbf{E}$, we arrive at the following final expression, which is denoted as Equation 2.15:

$$(j\omega\sigma - \omega^2 \varepsilon_0)\mathbf{A} + \nabla \times (\mu_0^{-1} \nabla \times \mathbf{A} - \mathbf{M}) = \mathbf{J}_e \tag{2.15}$$

Here, ω represents the angular frequency of $2\pi f$, ε_0 represents the permittivity of free space, μ_0 represents the permeability of free space, $\mathbf{M}$ denotes the magnetization of the material [38].

3 Experimental work

Throughout this section, the methodology for the experimental work performed during this thesis will be presented. The format for describing each experiment is consistent, starting with a comprehensive explanation of the experimental setup and test object, followed by a description of the testing procedure.

To begin with, this section will give an overview of the 50 Hz AC current experiments, followed by covering the switching transient and lightning impulse experiments. Lastly, it will give a thorough description of the process for conducting magnetic field simulations using COMSOL.

3.1 50 Hz AC current

The experiments involving 50 Hz AC current were carried out with two specific objectives in mind. The first objective was to measure the magnetic flux density generated by a high current travelling through a cable and compare it with computer simulation. The second objective was to investigate how the magnetic field affects the inductive partial discharge sensor based on inductive coupling, considering three different orientations and at a range of distances. This subsection will begin by providing a detailed explanation of the experimental setup and test object, followed by a thorough description of the testing procedure.

3.1.1 Experimental setup

The experimental setup for the 50 Hz AC current experiments can be explained by the circuit diagram presented in Figure 3.1. A complete table of all the equipment used during the 50 Hz AC current experiments can be found in Appendix A.1.

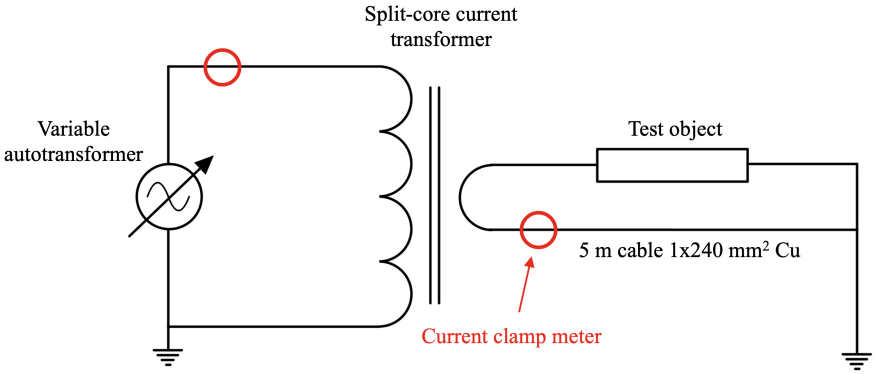

Figure 3.1: Circuit diagram of the experimental setup used during the 50 Hz AC current experiments.

On the primary side of the split-core current transformer, a variable autotransformer is used to apply the voltage. On the secondary side of the split-core current transformer, a short-circuited 240 mm^2 cable is threaded through the split-core current transformer and thus acting as a one-turn secondary winding. This will in turn generate a high current but with a low voltage. The dimensions of the cable are presented in Table 3.1.

Table 3.1: Dimensions of the low voltage supply cable with a copper conductor.

Outer radius		Cross section
Conductor [mm]	Insulation [mm]	Conductor [mm^2]
11.0	15.0	240

Given the short length of the 5-meter cable and it being short circuited, it is anticipated that a significant amount of current will flow through it, which could endanger both equipment and personnel. To mitigate these risks during experiments, two safety measures were put in place. Firstly, current clamp meters were employed to constantly monitor the current magnitude on both the primary and secondary sides of the split-core current transformer. Secondly, a thermal camera was used to monitor the temperature of the cable both for equipment and personnel safety.

In addition, a direct electrical connection between the cable and ground was established to enable self-discharge following a test cycle. Normally, this would cause a significant current to go directly to ground, however, it is feasible since the resistance to ground is considerably higher than the resistance of the short circuited cable, i.e., $R_{ground} \gg R_{cable}$. Consequently, during the actual testing, there will only be a small and insignificant current flowing to ground compared to the current in the conductor.

Test object

The test object consisted of the inductive partial discharge sensor, which inductively couples PD currents induced in the copper mesh through the use of a High-Frequency Current Transformer, as explained in Section 2.3. In an attempt to replicate the real-life conditions of a full-size outdoor oil-filled cable termination, the copper mesh was installed in accordance with the technical specifications provided for a 245 kV outdoor cable termination. Copper mesh with a thickness of 0.5 mm was wrapped around the cable in an overlapping manner equaling a total thickness of 1 mm and a total length of 0.7 m.

Subsequently, a 2 mm aluminium plate was placed beneath the copper mesh to simulate the termination's base plate. The aluminium base plate is grounded and the copper mesh connects directly to it from the cable. A photo of the described test object during the 50 Hz AC current experiment is presented in Figure 3.2.

Figure 3.2: Photo of the test object during the 50 Hz experiment. The test object consists of the inductive partial discharge through the use of a HFCT.

The High-Frequency Current Transformer used during the experiments was the Tekbox TBCP1-250 RF current monitoring probe, which is likely to be installed inside an actual oil-filled cable termination. This HFCT offers a usable frequency range from 10 kHz to 250 MHz [39]. The HFCT was placed on an adjustable stand to allow for easy manoeuvring between the tests performed. An equivalent circuit of the test object is presented in Figure 3.3.

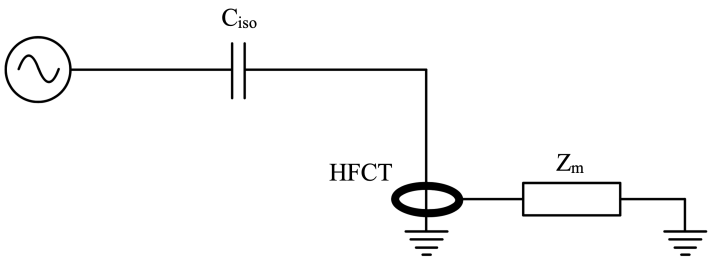

Figure 3.3: Equivalent circuit of the test object during the 50 Hz AC current experiments. C_{iso} is the capacitance of the cable insulation and Z_m is the measuring impedance, in this case internally in the oscilloscope.

Measurement setup

To measure the magnetic flux density generated and emitted by the cable, the GM08 Gaussmeter was used. The GM08 Gaussmeter is a hand-held unit with an LCD display which can do measurements of the magnetic flux density or the magnetic field strength. The Gaussmeter was equipped with a semi-flexible transverse probe.

The HFCT output voltage was measured using the Keysight DSOX2014A oscilloscope. The oscilloscope was primarily used to capture the voltage RMS value, but it was also used to analyze the voltage waveform. Based on an analysis of the voltage waveform, an assessment regarding if the HFCT ferrite core is undergoing saturation can be done, as explained in Section 2.5.4.

3.1.2 Tests performed

For the 50 Hz AC current experiments, two tests were performed in order to evaluate the magnitude of the magnetic field emitted from a cable and how it will interfere with the inductive partial discharge sensor. To begin with, the test for validation of the experimental setup will be explained followed by the effect of HFCT orientation and distance from cable.

Validation of the experimental setup

Initially, it was important to verify that the experimental setup corresponded to the analytical calculations and simulations. This was done through a simple comparison of the magnetic flux density measured at several distances from the cable. The parameters for the validation test are given in Table 3.2. It is worth noting that the test was conducted without the presence of the copper mesh, as it could marginally influence the measured field.

Table 3.2: Parameters used during the validation of the experimental setup test.

Parameter	Definition	Value
I	Applied current	1000 A
x	Distance from cable	5 - 150 mm

From Table 3.2, the magnetic flux density was measured at distances ranging from 5 to 150 mm away from the cable. The distance interval between successive measurements was incremented by 5 mm for each performed test. The positioning of the Gaussmeter's transverse probe was perpendicular and centred to the cable, as shown in Figure 3.4.

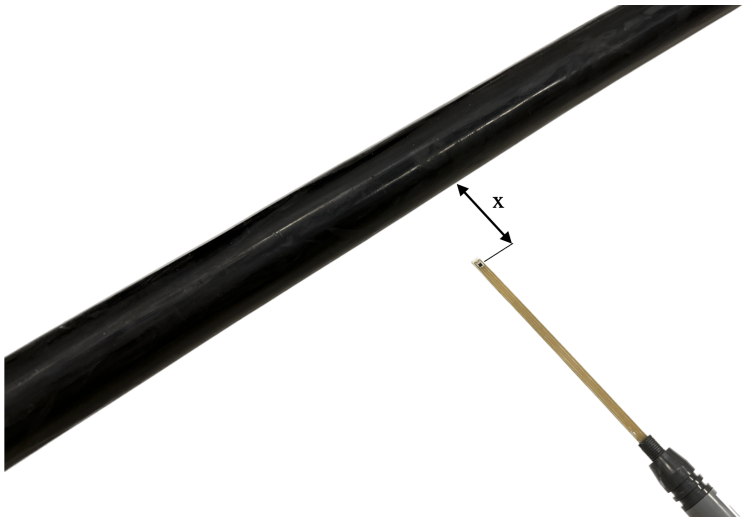

Figure 3.4: The positioning of the Gaussmeter during the validation testing. The probe is positioned perpendicular and centered to the cable with the possibility to adjust the distance.

Effect of HFCT orientation and distance from cable

The last 50 Hz AC current test performed involved investigating the influence of HFCT orientation and distance from the cable. As previously explained in Section 2.5.2 and shown in Figure 2.11, the magnetic field generated by a current-carrying cable will follow the right-hand rule. When a High-frequency Current Transformer is positioned in close proximity to the cable, it will become susceptible to the magnetic field due to the ferrite core's high permeability. The degree of susceptibility is also dependent on how the magnetic field interacts with the ferrite core.

Therefore, the orientation of the HFCT relative to the emitted magnetic field by the cable was assumed to have a crucial role in partial discharge detection and sensitivity. As a result, it was essential to conduct orientation tests on the HFCT to ensure its optimal performance. Based on practical experience during the installation of the HFCT within the termination housing, it was decided to proceed testing with the following three orientations:

- Orientation 1: Standing perpendicular with regards to the cable (Figure 3.5a)
- Orientation 2: Standing in parallel with regards to the cable (Figure 3.5b)
- Orientation 3: Laying flat with regards to the cable (Figure 3.5c)

(a) Orientation 1 **(b)** Orientation 2 **(c)** Orientation 3

Figure 3.5: The three different orientations tested for the HFCT with regards to the cable.

In order to achieve some uniformity between the orientations, the HFCT was positioned in the centre of the cable, in terms of height, for all three orientations. In addition to changing the HFCT orientations, tests varying the distance between the HFCT and cable were performed. The distance parameter ranged from 0 to 150 mm, where the interval between successive measurements was incremented by 10 mm.

The distance parameter was chosen based on the space available inside an oil-filled outdoor termination, as explained in Section 2.1. It should be noted that the distance parameter refers to the distance between the copper mesh on the cable and the HFCT casing, as shown in Figure 3.6.

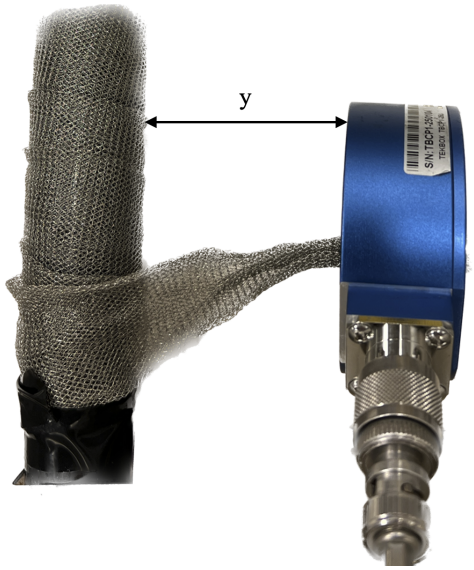

Figure 3.6: The distance testing of the HFCT, where the distance is between the applied copper mesh and the HFCT casing. Distance was measured with a calliper for higher precision.

The resulting output voltage from the HFCT was recorded through the oscilloscope and analyzed to quantify the impact that the distance and orientations have. The parameters used for the HFCT orientation and distance tests are given in Table 3.3.

Table 3.3: Parameters used for the HFCT orientation and distance tests.

Parameter	Definition	Value
I	Applied current	1000 A
y	Distance from cable	0 - 150 mm

3.2 Switching transients

The purpose of the experiments with switching transient was to investigate how a potential re-strike, current interruption and a large short circuit current will affect the inductive partial discharge sensor. This subsection will begin by thoroughly describing the experimental setup before specifying the tests performed.

3.2.1 Experimental setup

The diagram of the circuit used during the switching transient experiment is presented in Figure 3.7, and consists of a pre-setup configuration with the ability to adjust the component parameters. The component parameters were computationally calculated based on the objective of the experiment, which throughout this experiment was to have a high current amplitude.

The colours assigned to the test object, current and voltage measurement correspond to the resulting plots which will be presented in the following section. A complete table of all the equipment used during the switching transients experiment can be found in Appendix A.3.

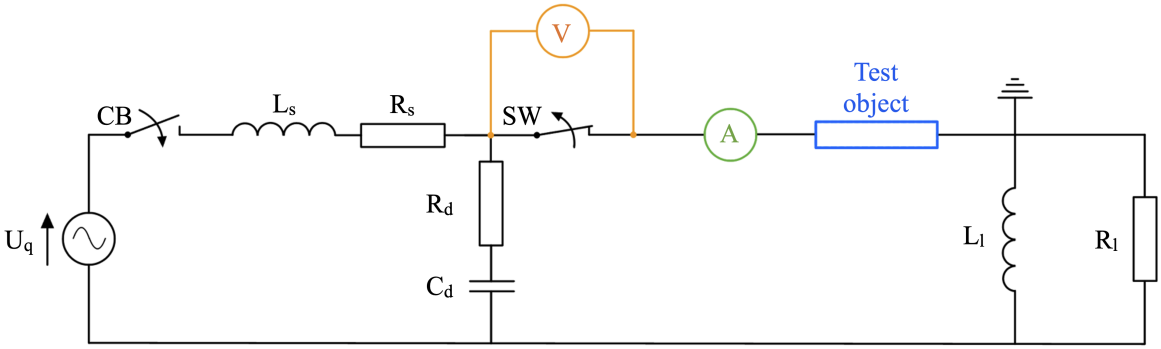

Figure 3.7: Circuit diagram of the setup for experiments with switching transients.

When initiating a test, the circuit breaker closes for 50 ms before opening and a short circuit current will flow through the test object. The switch breaker is only utilized when attempting to interrupt the current. The applied voltage, which is represented by the symbol U_q was set to 13.8 kV RMS.

The parameters of the circuit components are given in Table 3.4. The computed component parameters remained the same for all the tests performed, with the exception of when attempting to create a re-strike of the current arc. When attempting to create a re-strike, the capacitances were adjusted.

Table 3.4: Parameters of the circuit components used during the switching experiments.

Component parameters						
Component	L_s	R_s	R_d	C_d	L_l	R_l
Value	0.94 mH	0.11 Ω	1800 Ω	1 - 1.95 μF	30.35 mH	1.54 Ω

Test object

The test object consisted of the inductive partial discharge sensor attached to a two-meter long PEX insulated cable. The cable has a copper conductor and a voltage rating of 12 kV, with the dimensions presented in Table 3.5. The cable was initially received unprepared, i.e. cut through all its layers, and therefore had to be terminated prior to testing.

Table 3.5: Dimensions of the 12 kV PEX cable with a copper conductor.

Outer radius [mm]			
Conductor	Conductor screen	Insulation	Insulation screen
6.5	7.5	11.4	12.4

To begin the termination, the outer semi-conductor was removed approximately 33 cm at both ends and exposing the bare insulation. To make the end terminations with some electric field grading as explained in Section 2.1, IV termination tape was used. The termination tape was applied in an overlapping fashion, however, the number of overlaps varied on each side of the cable. The side where the copper mesh was to be applied on, was built up to represent the previously used stress cone, Nexans AIN Indoor slip-on termination. The other side only had two overlaps of termination tape.

After applying the termination tape, 70 cm of copper mesh was applied over the side where the termination tape was built up. After installing the terminated cable to the circuit, the High-Frequency Current Transformer was placed on a stand at a distance of 5 cm from the cable in orientation 1, as shown in Figure 3.8.

Figure 3.8: Terminated test object with applied termination tape and copper mesh. The copper mesh was applied over the termination tape and down the outer semi-conductor, to a total of 70 cm.

The HFCT orientation and distance from the cable remained the same throughout all the tests performed, based on two reasons. Firstly, the results obtained from 50 Hz AC current experiments revealed that orientation 1 was significantly better than the other orientations, in terms of how influenced it was by the magnetic field emitted by the cable. Secondly, each short circuit test performed in the laboratory has some economic impacts due to the degradation of the electrical components. As such, it was important to minimize the number of tests performed as the cost would not be worth it. Therefore, by keeping the HFCT orientation and distance from the cable constant, the testing process ensured both efficiency and cost-effectiveness.

The equivalent circuit for the test object consisting of a 12 kV PEX insulated cable with the inductive partial discharges attached is illustrated in Figure 3.9.

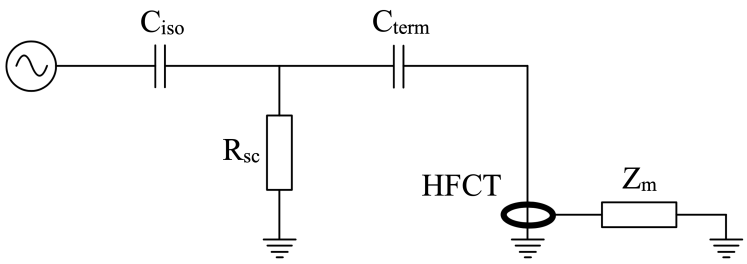

Figure 3.9: The equivalent circuit of the test object based on the inductive sensor and a 12 kV terminated cable. Where, C_{iso} is the capacitance of the cable insulation, R_{sc} is the stray resistance of the semiconductor, C_{term} is the capacitance of termination tape and Z_m is the measuring impedance.

Measurement setup

It was expected that significant voltage amplitudes could occur when measuring and recording the HFCT output voltage during the switching transient experiment. As a result, it was decided to use the Tektronix TDS 2014C oscilloscope, which is an inexpensive and basic oscilloscope for recording the HFCT output voltage. The oscilloscope was placed inside the high current laboratory, in close proximity to the test object.

For measuring the circuit current and voltage across the switch breaker, a Rhode & Schwarz RTB2004 oscilloscope was used. Both the Rhode & Schwarz and Tektronix oscilloscopes were configured to trigger on signals transmitted through fibre optic cables.

3.2.2 Tests performed

The following three tests were conducted for switching transients: Short circuit, current interruption by a switch breaker and current re-ignition.

Short circuit

To begin with, experiments with short circuit (SC) tests were performed. The main circuit breaker was engaged for 50 ms to allow a high current to circulate in the circuit. This experiment may resemble the 50 Hz AC high current experiment, however, the use of circuit breakers for current initiation was suspected to yield different results due to external noise from arcs. Also, it was interesting to see how a SC current with a DC offset would affect the inductive sensor. The switch breaker next to the test object was in the closed position during these experiments.

For the SC tests, two test configurations were carried out. The first SC test was with the CB engaging when the applied voltage is at zero, resulting in a SC current containing only the AC component. In the second SC test, the initiating of the main circuit breaker was delayed by 4 ms, causing a SC current with a higher amplitude and a decaying DC component. This is graphically presented in Figure 3.10.

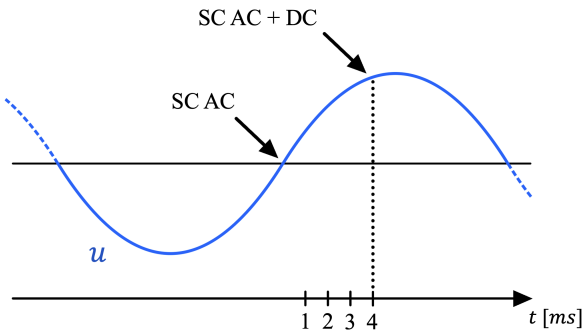

Figure 3.10: Illustration of the two SC tests performed. First, SC current contains only the AC component and secondly, the SC current contains both the AC and a decaying DC component.

Current interruption

The purpose of the current interruption tests is to evaluate how a switch breaker will affect the High-Frequency Current Transformer. Also, when attempting current interruption there may be a short-term current arc within the switch breaker chamber, which will release electromagnetic pulses within the HFCT frequency bandwidth.

Current interruption tests performed were done with the switch breaker (SW), indicated in Figure 3.7. The switch breaker was initiated 10 ms after energizing the circuit through the use of the circuit breaker, as shown in Figure 3.11. The SC has a duration of 50 ms, leaving the SW with three consecutive CZ crossings to interrupt the SC current.

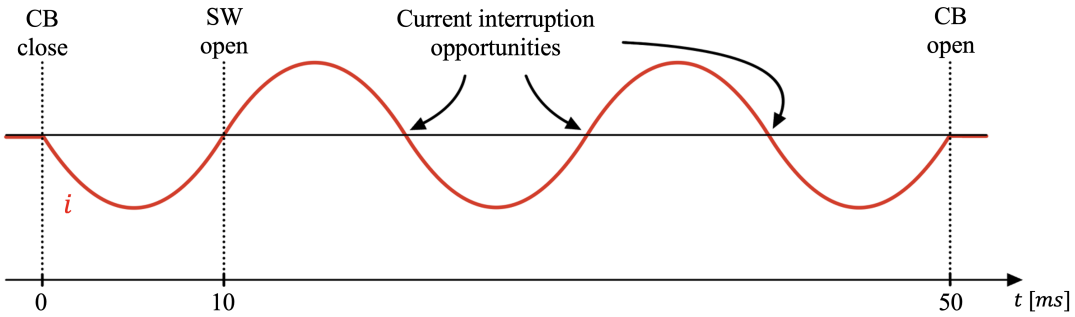

Figure 3.11: The short circuit current with timestamps of breaker and switcher activity during current interruption tests.

Current re-strike

The purpose of the current re-strike experiment was to create a fast-acting transient current, di/dt, as explained in Section 3.2. In attempts to achieve a re-strike, multiple current interruption tests as shown in Figure 3.11 were conducted. However, now the circuit capacitances were adjusted between each test.

By adjusting the capacitances, it becomes possible to discretely tune the current interruption process, such that the system operates on the verge between successful and unsuccessful current interruption, thereby increasing the chances of a re-strike.

3.3 Lightning impulses

Lightning impulses are characterized as very fast-acting transients and thus will produce a fast-acting magnetic field around the cable. This fast-acting magnetic field is assumed to affect the inductive partial discharge sensor given the frequency bandwidth it offers. This subsection will start by giving a description of the experimental setup before explaining the test procedure.

3.3.1 Experimental setup

The experimental setup can be explained through the simplified circuit diagram presented in Figure 3.12. The colours assigned to the test object, current and voltage measurements correspond to the resulting plots, which will be presented in Section 4.3.

A complete list of all the equipment used during the lightning impulse experiment can be found in Appendix A.3.

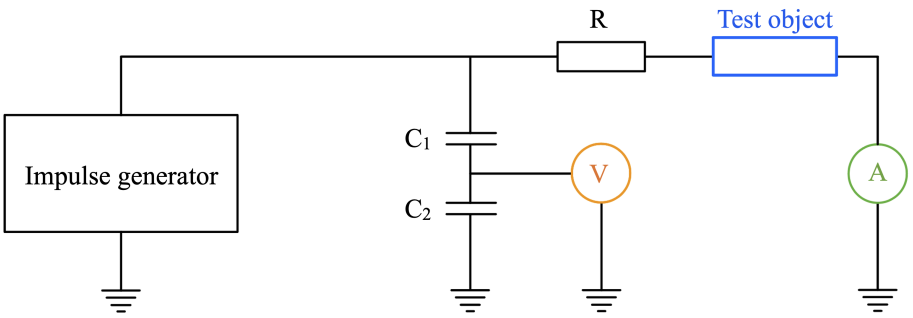

Figure 3.12: Circuit diagram for the lightning impulse experiments.

Starting on the left-hand side, the impulse generator is made up of the "HighVolt Impulse Voltage Test System" which has the ability to generate an impulse voltage of up to 1.2 MV, or 100 kV per stage. Each stage has a charging energy of 5 kJ and an impulse capacitance of 1000 nF. However, for the experiments to be conducted in this thesis it was sufficiently with a maximum of two stages.

A capacitive voltage divider is used to take measurements of the applied voltage during the lightning impulse. On the right-hand side of the circuit diagram, the test object is in series with current measurement and a resistor. The size of the resistor was chosen according to the desired current magnitude and front-time. The parameters for the components shown in Figure 3.12 are presented in Table 3.6.

Table 3.6: Parameters of the components used during the lightning impulse experiments.

Component values				
Component	U_i	C_1	C_2	R
Value	40-200 kV	1.33 nF	1.33 nF	515 Ω

Test object

The test object during the lightning impulse experiment remained the same as in the previous switching transient experiment.

A two-meter long PEX insulated cable with the inductive partial discharge sensor attached, as shown in Figure 3.13. The only difference made to the previous experiment was that the test object now did not contain the 2 mm aluminium base plate due to difficulties installing it.

The HFCT orientation and distance from the cable remained constant during the entire lightning impulse experiment, based on the same reasons explained for switching transients. The HFCT was positioned in orientation 1 and at a distance of 5 cm away from the cable.

Figure 3.13: Photo of the test object taken in the laboratory. The equivalent circuit of the test object remains the same as during the switching transient experiment, previously presented in Figure 3.9.

Measurement setup

To measure the current of the lightning impulse, a current probe 94606-1 was clamped around the 12 kV cable in the test object. Once again, the Tektronix 2014 oscilloscope was utilized to capture the waveform from the current probe and HFCT.

Triggering of the oscilloscope was done through manually set trigger levels. It was expected that high voltage amplitudes could occur, which may cause damage to the oscilloscope, therefore modifications were done to the HFCT and current probe. The HFCT was equipped with a 20 dB attenuator, whereas the current probe was equipped with 26 dB of attenuators. In addition, both the HFCT and current also had 50 Ω end terminations.

3.3.2 Tests performed

The main objective of the experiments with the lightning impulses was to see how the proposed partial discharge sensor based on inductive coupling responded to a very fast-acting transient magnetic field. As a result, the test regime for this experiment was rather simple. The voltage magnitude of the lightning impulses was increased until noticeable readings on the HFCT output voltage were made.

Preliminary impulse testing was conducted at voltage levels of 6, 10, and 20 kV. The results revealed a voltage relationship of 0.65 between the applied and measured voltage across the resistance and test object. Consequently, when applying a 10 kV lightning impulse, the measured voltage amplitude across the resistor and test object was found to be 6.5 kV. This voltage relationship remained constant even when the applied voltage was adjusted. Hence, it was possible to determine the current amplitude through the test object using the following analytical equation:

$$\mathrm{I} = \frac{\mathrm{U}_{applied} \cdot 0.65\ \mathrm{V}}{515\ \Omega}\ [\mathrm{A}] \tag{3.1}$$

Considerations of the resistance and inductive to the laboratory grounding system have been made, however, it becomes negligible when comparing it to the 515 Ω resistor and as a result is not considered in the calculations.

Four lighting impulse tests will be presented in the following section, with the applied voltage set to 40, 80, 160 and 200 kV. The resulting lightning impulse current amplitudes are calculated using Equation 3.1 and are presented in Table 3.7. In addition, each of the four lighting impulse tests has been assigned a test name that will be used when presenting the results.

Table 3.7: The applied voltage, analytically calculated current based upon preliminary testing and the names for the lightning impulse tests to be performed.

$\mathbf{U}_{applied}$	**Current**	**Test name**
40 kV	50.5 A	40 kV - 50 A
80 kV	100.1 A	80 kV - 100 A
160 kV	200.2 A	160 kV - 200 A
200 kV	252.4 A	200 kV - 250 A

Each stage of the "HighVolt Impulse Voltage Test System" has the ability to charge up to 100 kV. As a result, only one stage was used for the first two tests at 40 and 80 kV. For the remaining two lightning impulses at 160 and 200 kV, two stages were utilized.

3.4 Magnetic field simulations

The purpose of the magnetic field simulations was mainly for comparison to the 50 Hz AC current experiments conducted, but also to lay the foundation for further simulations. This subsection will begin by explaining how the simulation for validating the magnetic flux density was done. Finally, it will give a description on how the simulations to evaluate HFCT orientation and distance from cable were carried out.

3.4.1 Validation of the experimental setup

The 3D magnetic field model made in COMSOL for the validation of the experimental setup was made in accordance with how the 50 Hz AC current experiments were conducted. The cable was modelled according to dimensions given in Table 3.1, however, the cable insulation was neglected as it will not have any impact on the magnetic field simulations. Figure 3.14 presents a graphical illustration of the 3D model created in COMSOL.

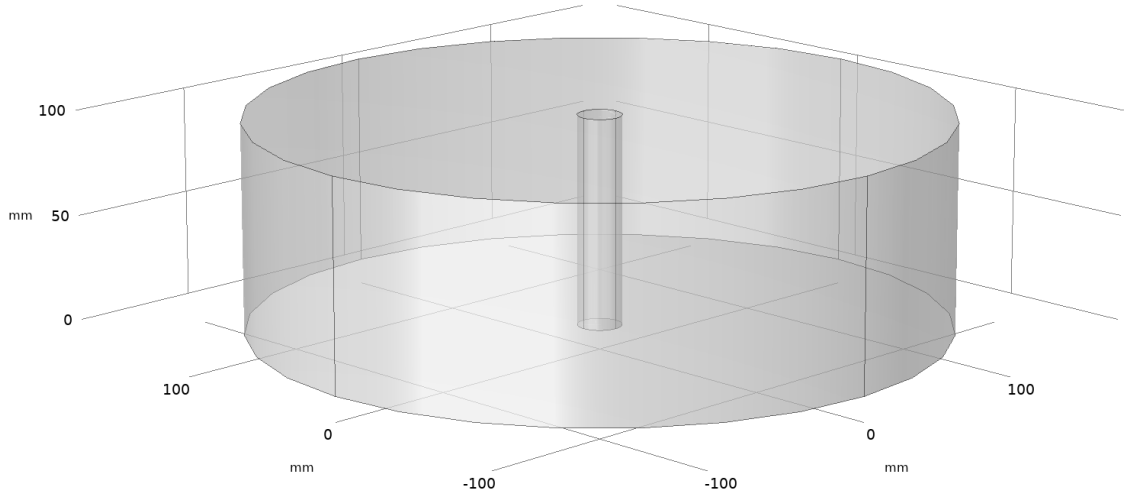

Figure 3.14: An illustration of the 3D model made for validating the experimental setup. Only the materials with magnetic properties are modelled, which in this case is the conductor.

Further, the boundary conditions of the validation model are presented in Figure 3.15. The cable conductor and air were modelled with continuity at both the top and bottom planes, implying that they are infinitely long. The outer walls of the air were modelled with magnetic insulation, which acts as a ground plane and sets the magnetic potential to zero.

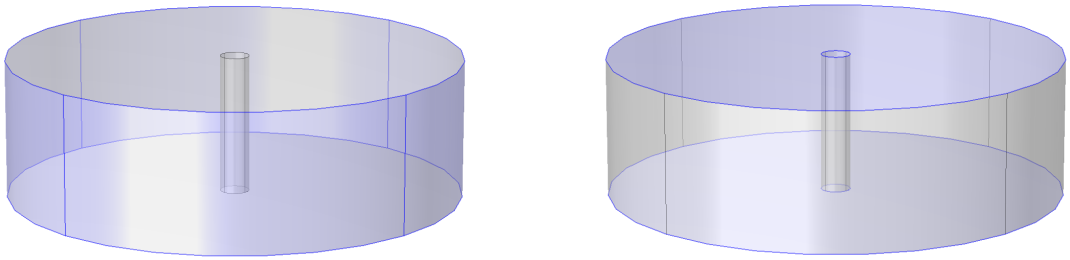

(a) Magnetic insulation **(b)** Periodic condition - Continuity

Figure 3.15: Graphical representation of the set boundary conditions for the validation model. The outer walls of the modelled air are set to magnetic insulation, whereas the top and bottom is set to continuity through periodic condition.

The conductor was modelled as copper with 1000 A of applied current travelling through it, at the network frequency of 50 Hz. All the relevant parameters used during the simulation of the validation model are presented Table 3.8. When a successful simulation was performed, then the magnetic flux density is evaluated through a perpendicular 3D cut line from the cable.

Table 3.8: Simulation parameters for applied current, conductor and air radius for the validation of the experimental setup simulation in COMSOL.

Parameter	Definition	Value
I	Applied current RMS	1000 A
f	Frequency	50 Hz
r_c	Conductor radius	11 mm
r_a	Air radius	165 mm

3.4.2 Effect of HFCT orientation and distance from cable

To evaluate the effect of HFCT orientation and distance from cable in COMSOL it was decided to only pursue with two orientations, 1 and 2. This decision was based on the results gathered from the initial 50 Hz AC current experiments, which revealed that orientation 1 is the best and orientation 2 is the worst in terms of induced output voltage from an adjacent magnetic field generated by a cable.

The purpose of this magnetic field simulation was to compare it to the obtained values gathered during the 50 Hz AC current experiment. To achieve comparable values, the model had to be created to replicate the real setup. As a result, in addition to the cable conductor, it involved constructing the copper mesh, High-Frequency Current Transformer (HFCT) and threading the copper mesh wire through the HFCT. This had to be done for two unique 3D models in COMSOL and a graphical illustration of both models are illustrated in Figure 3.16

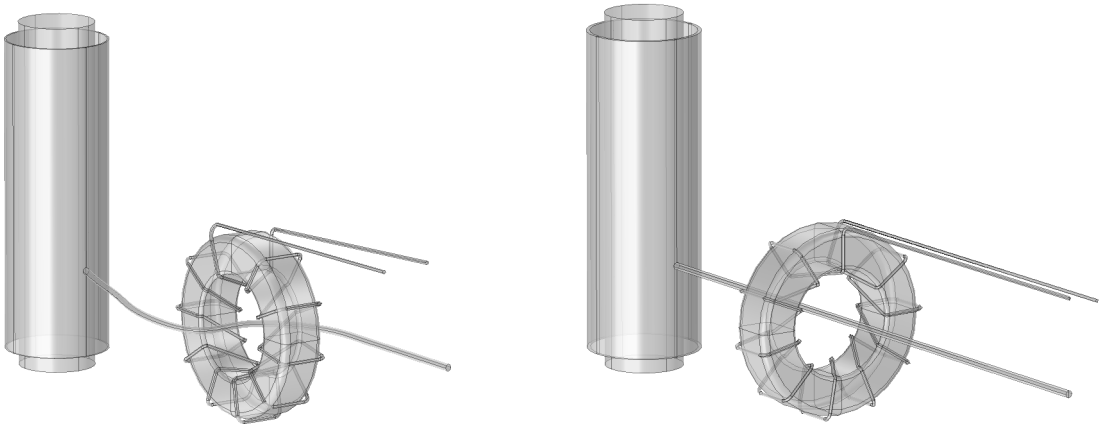

(a) Orientation 1 - 3D model COMSOL **(b)** Orientation 2 - 3D model COMSOL

Figure 3.16: Graphical representation of the 3D models made in COMSOL for HFCT orientation 1 and 2. It now contains the copper mesh and the HFCT.

Following, the boundary conditions of the models are presented in Figure 3.17. Similarly to the validation model, the outer walls of the air are set to magnetic insulation, which sets the magnetic potential to zero and works as a ground plane. The top and bottom model planes, including the air and conductor, was set to periodic condition with continuity, implying that both the conductor and air are infinitely long.

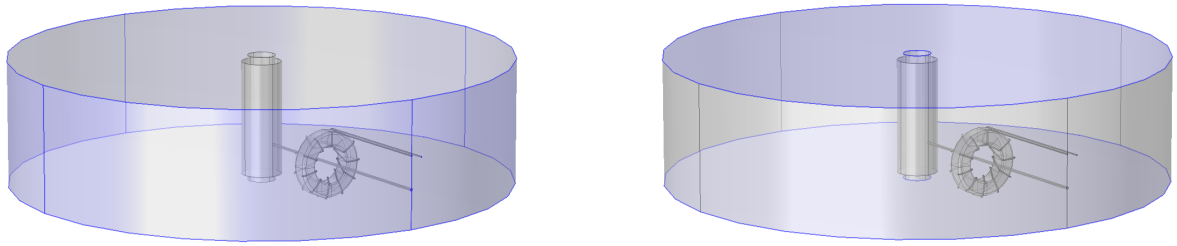

(a) Magnetic insulation **(b)** Periodic condition - Continuity

Figure 3.17: Graphical representation for the set boundary conditions. The outer walls of the modelled air are set to magnetic insulation, whereas the top and bottom is set to continuity through periodic condition.

To extract voltage values from the modelled HFCT after a successful simulation, a combination of the magnetic field and electrical circuit physics had to be used. To begin with, the ferrite core was modelled based on actual measurements and a separate Ampère's Law calculation has to be performed for it. From the Ampère's Law calculation, a magnetization model with a standard effective B-H curve derived from the material properties was used.

Finally, the HFCT winding must be equipped as a coil, where the coil excitation is generated by the circuit current, which then is connected to the electrical circuit physics. In the electrical circuit physics, the coil excitation current will be transformed into a voltage source, thus allowing the extraction of voltage values.

The meshing of the models was done through physics-controlled meshing at an element size of finer. Although some preliminary simulations were carried out with even finer meshing, the trade-off in accuracy compared to simulation time proved to not be worth it. Illustration of the constructed meshing for orientation 2 can be seen in Figure 3.18. The number of elements differed slightly depending on the models and positioning but were in the range between 192434 and 242620.

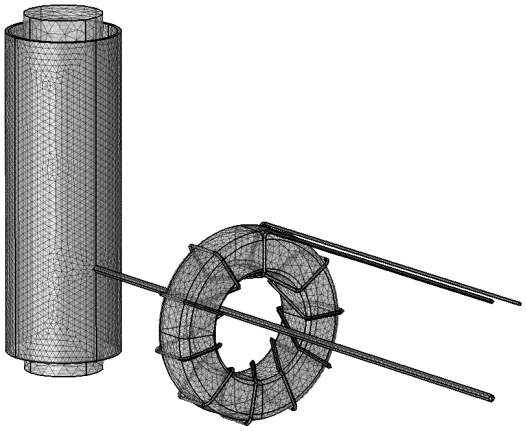

Figure 3.18: Illustration of the constructed mesh within COMSOL for orientation 2. Meshing was done through physics-controlled meshing at an element size of finer.

As a final remark, it was important to consider that during the distance experiments conducted in the laboratory, the HFCT was positioned in relation to the copper mesh. Meanwhile, the models made in COMSOL only include the ferrite core and winding. To address this discrepancy, manual measurements were conducted inside the HFCT casing, revealing a 7 mm distance between the outer casing and the ferrite core. This measurement was factored into the simulations accordingly.

The magnetic field simulation parameters, including their definitions and values, for the HFCT orientation and distance are given in Table 3.9. For simulating the distance ranging from 0 to 150 mm, parametric sweeping was used with an interval of 10 mm.

Table 3.9: Simulation parameters used during the HFCT orientation and distance simulations in COMSOL.

Parameter	Definition	Value
I	Applied current RMS	1000 A
f	Frequency	50 Hz
r_c	Conductor radius	11 mm
r_{mesh}	Copper mesh radius	15 mm
d_{mesh}	Copper mesh thickness	1 mm
μ_{mesh}	Permeability copper	1
μ_{core}	Permeability HFCT core	2000
y	Distance from cable	0 - 150 mm

4 Results

This section will present the results from the conducted experiments and simulations explained in Section 3, and will follow the same structure. It will start by presenting the results from the 50 Hz AC current experiments before presenting the results from the switching transient and lightning impulse experiments. Finally, the results from the magnetic field simulations in COMSOL will be presented. Throughout the section, the key findings will be briefly discussed.

4.1 50 Hz AC current

In this subsection, the results from the 50 Hz AC current experiments, described in Section 3.1, will be presented. It will begin by presenting the findings from the validation of the experimental setup before progressing to the results obtained from the HFCT orientation and distance tests.

4.1.1 Validation of the experimental setup

The purpose of the validation of the experimental setup was to ensure that the measured magnetic flux density in the experiments adhered to the simulations and analytical calculations. If the magnetic flux density measurements align with the simulations and calculations, it could lay the foundations for further analysis through simulations.

In Figure 4.1, a line plot of the measured magnetic flux density from the experiments at distances ranging from 5 to 150 mm is shown. The current through the cable was kept at 1000 A while the magnetic flux was measured in intervals of 5 mm. All the measurements can be found in Table D.1 coloumn 2 in Appendix D.

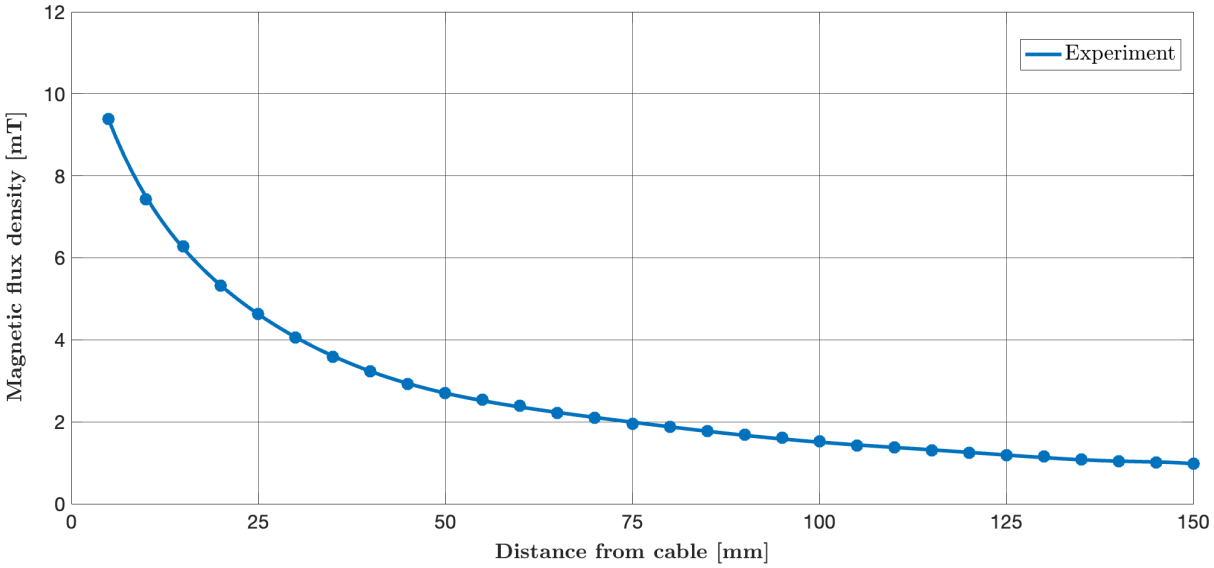

Figure 4.1: Line plot of the measured magnetic flux density during the 50 Hz AC current experiments with the use of GM08 Gaussmeter. The testing distances ranged from 5 to 150 mm from the cable, with a measurement interval of 5 mm. The current through the cable was kept at 1000 A.

The measured magnetic flux density starts at 9.38 mT before decreasing inversely proportionally. This is in line with the theory presented in Section 2.5.2, where the magnetic flux density from a current carrying conductor will decrease inversely proportional at a rate of $\frac{1}{r}$. The measured magnetic flux density will be further discussed in the following section, through a magnetic flux density comparison between the experimentally obtained, magnetic field simulations in COMSOL and analytical calculations.

4.1.2 Effect of HFCT orientation and distance from cable

Line plots of HFCT output voltage as a function of distance from the cable for each of the three HFCT orientations are presented in Figure 4.2. The voltages are expressed as RMS values. The measurements were conducted at distances ranging from 0 to 150 mm with an interval of 10 mm and the applied current through the cable was set to 1000 A.

A complete table of all the experimentally obtained output voltage from the orientation and distance testing can be found in Appendix B.

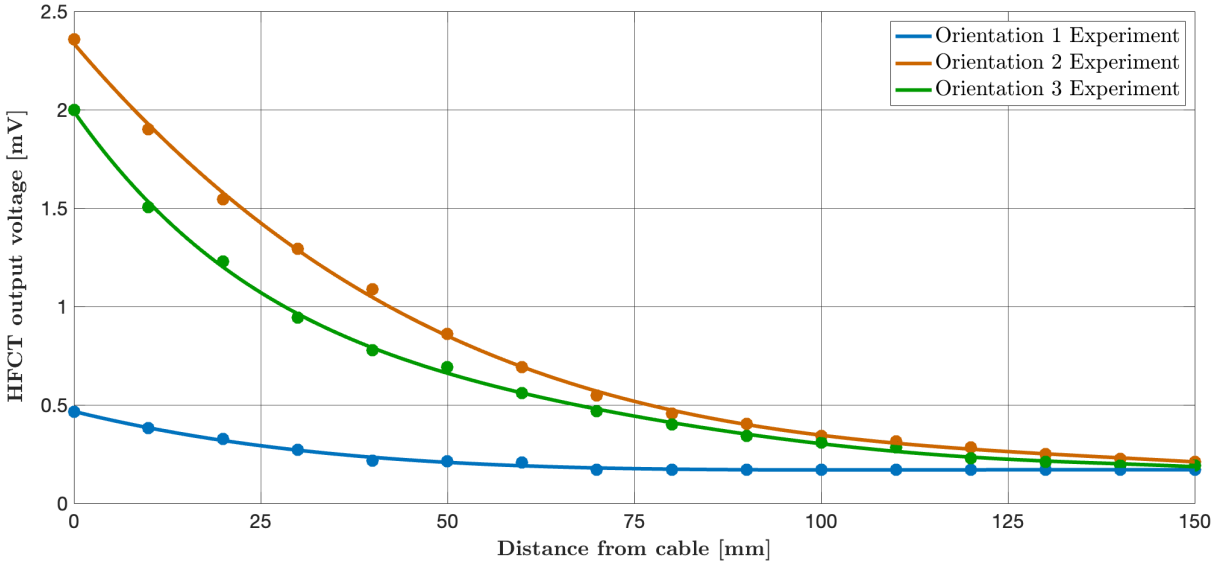

Figure 4.2: Line plots of the measurement of the induced RMS voltage in the HFCT for all three orientations as a function of distance from cable. The cable current was set to 1000 A for all measurements and the voltage is expressed in RMS.

From the presented line plots, it can immediately be observed that orientation 1 induces a significantly lower output voltage than orientations 2 and 3. In terms of performance for the inductive partial discharge sensor, a lower induced voltage is desirable as it indicates that the magnetic field does not significantly impact the sensor. As a result, orientation 1 becomes the preferred HFCT orientation when installing it within the cable termination housing.

The line plot for orientation 1 shows a descending curvature from its peak value of 0.46 mV until reaching 75 mm, where it remains constant at 0.17 mV. This reflects the point during the measurements when the induced external noise produced by nearby electrical equipment exceeded the induced voltage by the magnetic field. Therefore, it is unknown how low the voltage would have been at distances greater than 75 mm in a noise-free environment, but it is expected that it will continue to follow the previous downward curve towards zero.

Further, orientation 2 induces the highest output voltage among all three orientations, making it the least preferred orientation. The curvature of the line plot for orientation 2 shows an inversely proportionally descending form, having similarities with how the magnetic flux density decreases with distance. Orientation 3 nearly induces just as high of an output voltage as orientation 2, with the same descending curvature. This makes orientation 3 the second worst.

However, at the maximum testing distance of 150 mm from the cable, the variation in HFCT output voltage between all three orientations becomes small. It is assumed that the output voltage would stabilize at 0.17 mV for all orientations after 150 mm due to the explained external noise.

Lastly, when measuring the magnitude of the HFCT output voltage through an oscilloscope, an interesting observation was made regarding the waveform of the voltage.

Waveform of the output voltage

Figure 4.3 presents the voltage waveform at a distance of 0 mm from the cable with 1000 A of current through the cable. The vertical voltage scale for all the scope images are set to 2 mV/square. The very fast voltage spikes observed for all three orientations, but most prevailing for orientation 1, are assumed to originate from external noise.

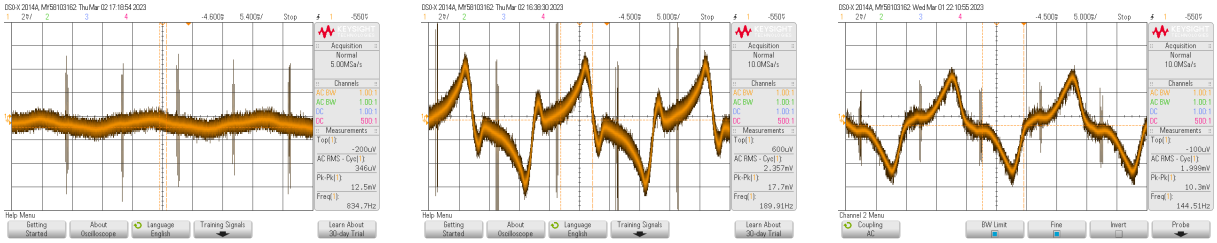

Orientation 1 - 0 mm | Orientation 2 - 0 mm | Orientation 3 - 0 mm

Figure 4.3: Scope images of the output voltage waveform from HFCT at a distance of 0 mm from the cable.

Analysis of the scope images at a distance of 0 mm from the cable reveals that the output voltage of the HFCT is severely distorted in orientations 2 and 3. This behaviour is a common characteristic feature of a transformer upon reaching saturation, as previously explained in Section 2.5.4. A potential core saturation of the HFCT caused by a 50 Hz magnetic field will reduce its sensitivity to detect partial discharges over its entire frequency bandwidth [7].

In comparison, Figure 4.4 presents scope images taken of the voltage waveform at a distance of 100 mm with the same 1000 A of current through the cable. The vertical voltage scale also remained the same at 2 mV/square.

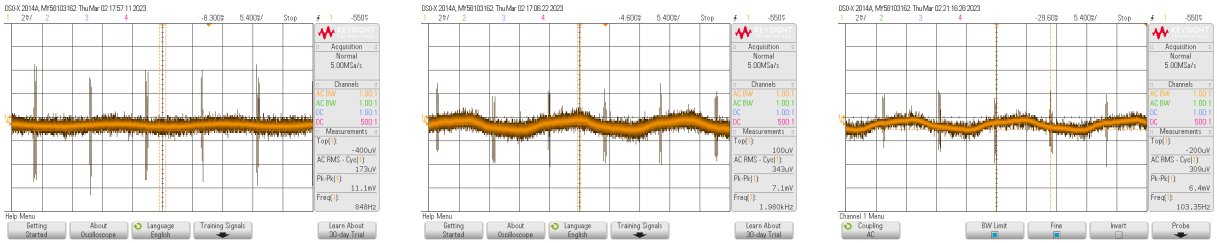

Orientation 1 - 10 mm | Orientation 2 - 10 mm | Orientation 3 - 10 mm

Figure 4.4: Scope images of the output voltage waveform from HFCT at a distance of 10 mm from the cable.

At an HFCT distance of 100 mm from the cable, the voltage distortion present at 0 mm is no longer visible for neither orientation 2 nor 3. This indicates that the ferrite core no longer is saturated. A collection of scope images for all three orientations at distances ranging from 0 to 100 mm can be found in Appendix C, which unsurprisingly reveals that an increase in distance reduces the voltage waveform distortion and thus core saturation.

4.2 Switching transients

Throughout this subsection, the results from the switching transient experiments will be presented. It will begin by presenting the result from the short circuit tests before progressing to presenting the results gathered from the current interruption and current re-strike tests.

The results will be presented as line plots of the scope images recorded during the experiments. The dampening of the used attenuators has been factored into the presented plots and the colour schemes of the presented line plots correlate to the circuit diagram for the switching experiments presented in Figure 3.7.

4.2.1 Short circuit

Two short circuit tests were performed, one where the SC current only contains the AC component and the other with both the AC and a decaying DC component. Preliminary short circuit tests were conducted without the inductive partial discharge installed and the resulting SC current without a decaying DC component was found to have a RMS value of $\sim$ 1050 A.

To begin with, the test where the short circuit current only contains the AC component will be presented through Figure 4.5. It presents the scope images of the HFCT output voltage in blue and the SC current in green.

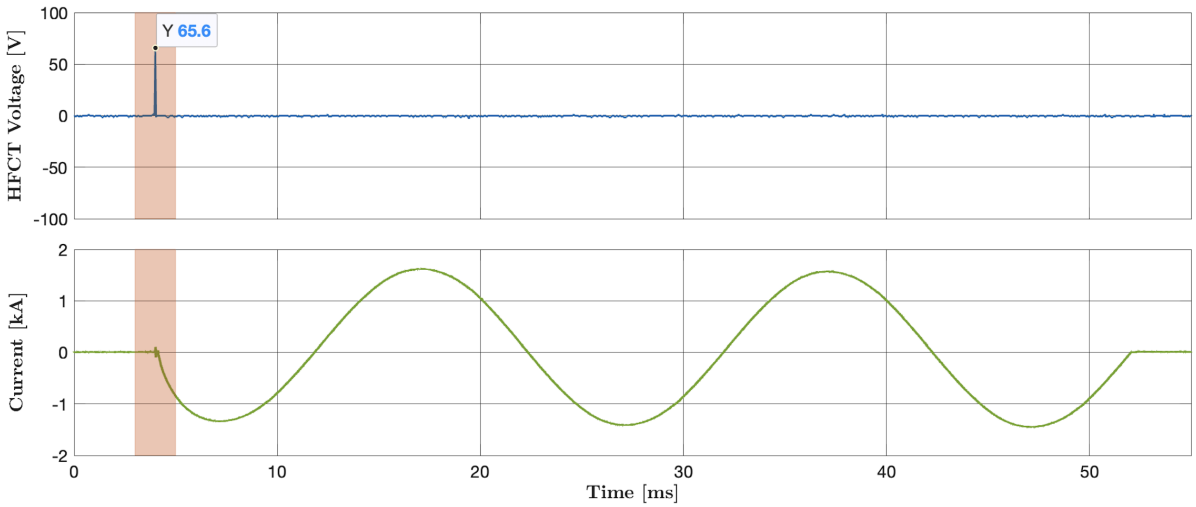

Figure 4.5: Scope images of the HFCT output voltage and SC current. The maximum HFCT output voltage was found to be 65.6 V. The red transparent area indicates where the initiation of the main circuit breaker occurs.

As observed in Figure 4.5, the inductive partial discharge sensor does not get largely affected by the short circuit current itself. However, in the transparent red area, an induced voltage spike of 65.6 V was detected and it occurs during the initiation of the main circuit breaker. It is suspected that the voltage amplitude can be even higher due to the low sampling rate provided of the oscilloscope used. Voltages with such a high amplitude can pose a threat to sensitive partial discharge measuring systems, necessitating the need to establish appropriate forms of protective measures.

Next, a SC current containing both an AC and a decaying DC component was performed to evaluate the impact it had on the HFCT output voltage. The results of the induced HFCT voltage and circuit current are presented in Figure 4.6. One important remark about the presented plot is that the induced HFCT voltage now is in mV, in order to capture the DC-offset present through the HFCT output voltage.

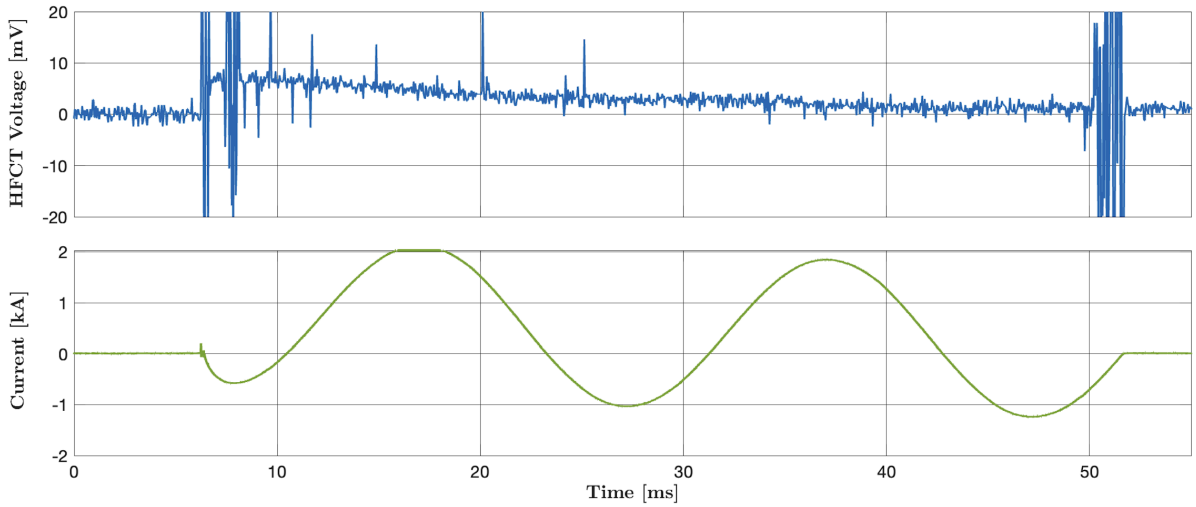

Figure 4.6: Scope images of HFCT output voltage and the SC current with a decaying DC component.

From Figure 4.6, it is evident that the HFCT detects the decaying DC component of the SC current, however, it is negligible compared to the maximum voltage amplitude of 65.6 V caused by breaker initiation presented in Figure 4.5. The voltage spikes caused by the main circuit breaker activity also seem to be present in this plot, but the amplitude remains unknown due to the scaling used.

4.2.2 Current interruption

The current interruption was done by initiating the switch breaker 10 ms after closing the main circuit breaker. Figure 4.7 presents the resulting induced HFCT voltage, circuit current and voltage over the switch breaker during a late current interruption by the SW.

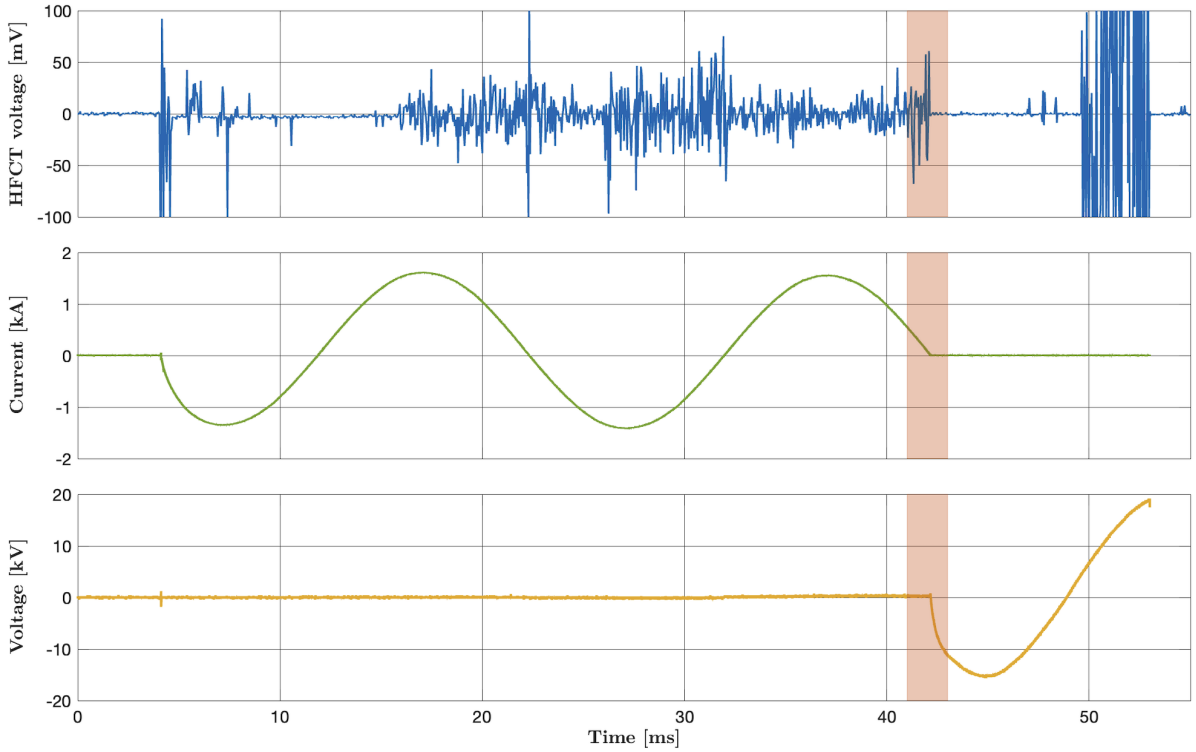

Figure 4.7: Scope images of HFCT output voltage, current in the circuit and voltage over the breaker during a late current interruption. The transparent red area indicates where the current was interrupted.

As observed in Figure 4.7, the high voltage amplitudes due to closing and opening of the main circuit breaker are still present. Looking away from these, the current is interrupted at the last CZ crossing at around 43 ms. The resulting HFCT output voltage due to current interruption is found to have an amplitude of 60 mV.

More interestingly, it can be seen from the HFCT output voltage that the switch breaker is activated at around 17 ms. As a result, the following CZ crossings result in higher HFCT output voltage amplitudes. This is assumed to be a result of electromagnetic pulses released from the current arc extinguishing and ignition within the switch breaker during a current zero passing.

The highest HFCT voltage amplitude, when still ignoring circuit breaker activity, is found to be at the CZ crossing at 23 ms with an unknown voltage amplitude. It is however assumed that this voltage amplitude is lower than the previously presented maximum output voltage of 65.6 V caused by circuit breaker initiation. This assumption is based on that the following CZ crossing only produced a HFCT output voltage of 75 mV.

A number of current interruption attempts where conducted, and Figure 4.8 shows the HFCT output voltage, circuit current and voltage over the switch breaker for an earlier current interruption.

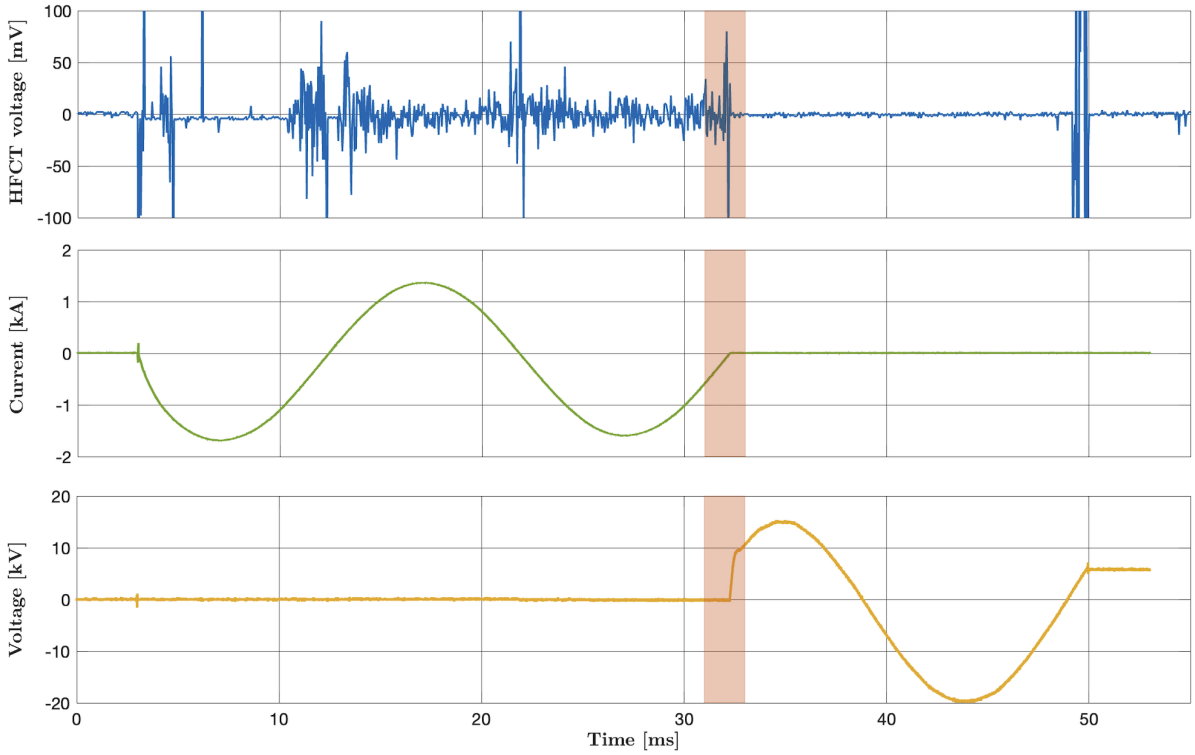

Figure 4.8: Scope images of HFCT output voltage, current in the circuit and voltage over the breaker during an early current interruption. The red area indicates where the current was interrupted.

The presented scope image in Figure 4.8 shows similar results as for the late current interruptions, where the highest voltage amplitudes occur at the CZ crossings. The voltage amplitudes seem to be somewhat higher, however they are still assumed to be significantly lower than the maximum HFCT voltage due to initiation of the main CB.

A closer inspection of the HFCT output voltage reveals that the switch breaker now has been activated earlier than in the previous current interruption. As a result, it provided an additional CZ crossing for current interruption at 13 ms which likely is the reason for the earlier current interruption.

4.2.3 Current re-strike

A number of attempts for current re-strike were attempted through the method of adjusting the circuit capacitances as explained in Section 3.2. However, no properly successful current re-strikes were achieved. Figure 4.9 shows the line plots of an attempt where a current re-strike nearly happened.

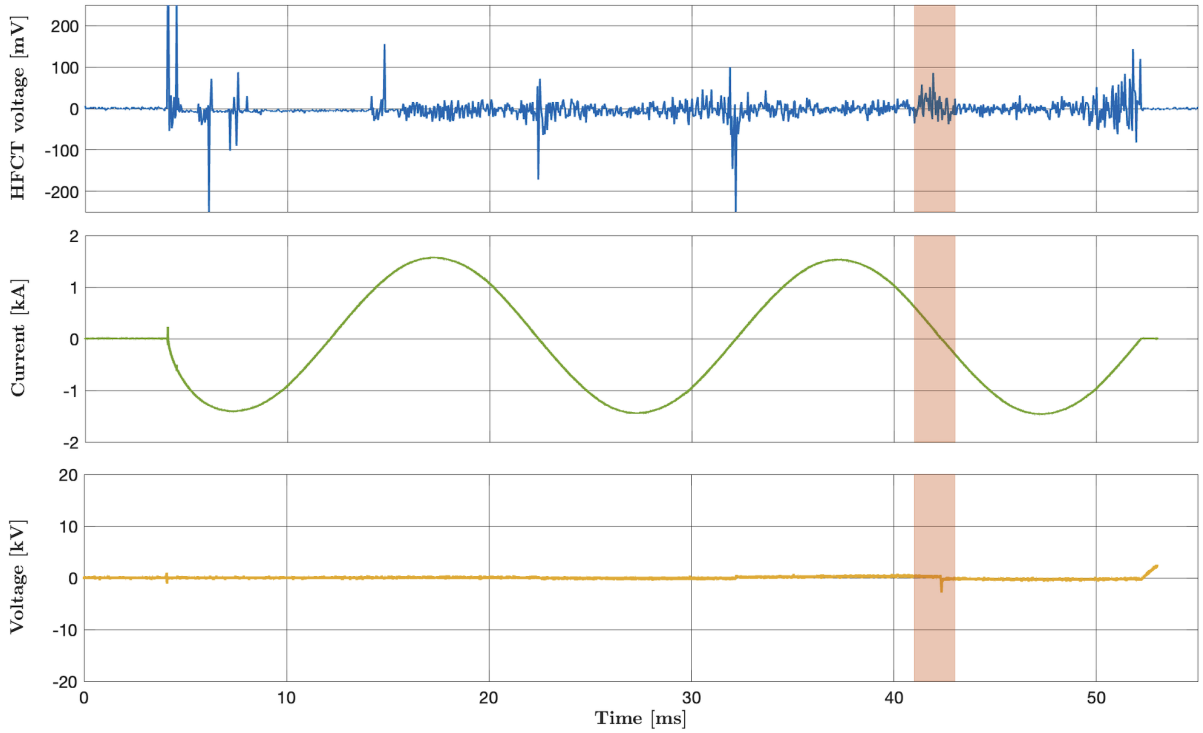

Figure 4.9: Scope images of HFCT output voltage, current in the circuit and voltage over the breaker during a near current re-strike attempt. The red transparent area indicates where the current re-strike nearly occurred.

The red transparent area indicates where the re-strike nearly took place. It is evident that the voltage over the switch increased to roughly 3 kV, indicating that the current arc was nearly extinguished. However, the current plot shows that the current remained unaffected by this voltage spike. Some activity is observed for the HFCT output voltage, with a peak value of 90mV, however, it becomes negligible when comparing it to the previous maximum HFCT voltage caused by CB initiation.

After 20 unsuccessful attempts for a current re-strike, it was decided to not pursue it any further.

4.3 Lightning impulses

This subsection will present the results gathered from the lightning impulse experiments described in Section 3.3. The lightning impulse tests will be presented in the following chronological order: 40 kV - 50 A, 80 kV - 100 A, 160 kV - 200 A, and 200 kV - 250 A.

The results will be presented as processed scope images recorded during the experiment. The dampening of the used attenuators and end-terminations was factored into the plots accordingly. The colour schemes of the scope images correlate to the circuit diagram for the lighting impulse experiment presented in Figure 3.12.

4.3.1 40 kV - 50 A

The presented scope images in Figure 4.10 present the HFCT output, current through the test object and measured voltage for the 40 kV - 50 A lightning impulse test. The voltage front-time, T_1, achieved remained identical for all experiments at 1 μs and the half-value time, T_2, was 44 μs.

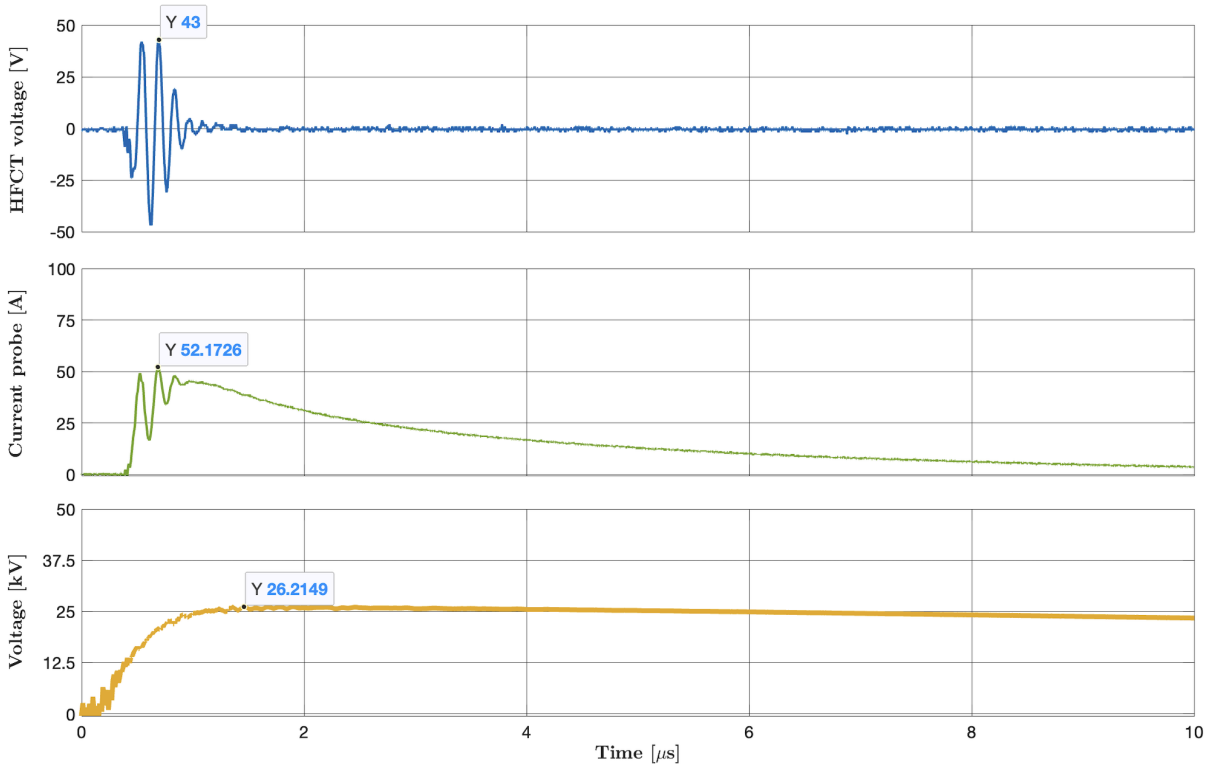

Figure 4.10: Scope images of HFCT output voltage, current measurement and the applied voltage for a 40 kV lightning impulse.

As observed in Figure 4.10, the scope image from the HFCT reveals a highly oscillating voltage with a peak value of 43 V. This does not resemble an exponential impulse current form, as explained in Section 2.4.1. It is assumed that it originates from the initial spark gap generated by the impulse generator. There may be a small exponential impulse current waveform, but the magnitude of the oscillations seems to overshadow it.

By inspecting the current probe curvature, it seems to have more of the expected exponential impulse current waveform with a peak value of 52.2 A. However, it also seems to detect the initial spark from the impulse generators as it contains similar oscillations as is present for the HFCT. The applied voltage was set at 40 kV, but the measured voltage across the 515 Ω resistor and test object was measured to be 26.2 kV. As a result, the relationship between the applied voltage and obtained voltage is found to be 0.66.

4.3.2 80 kV - 100 A

The applied voltage and current are now double to 80 kV - 100 A, and the resulting scope images of the HFCT output voltage, current measurement and measured voltage are presented in Figure 4.11.

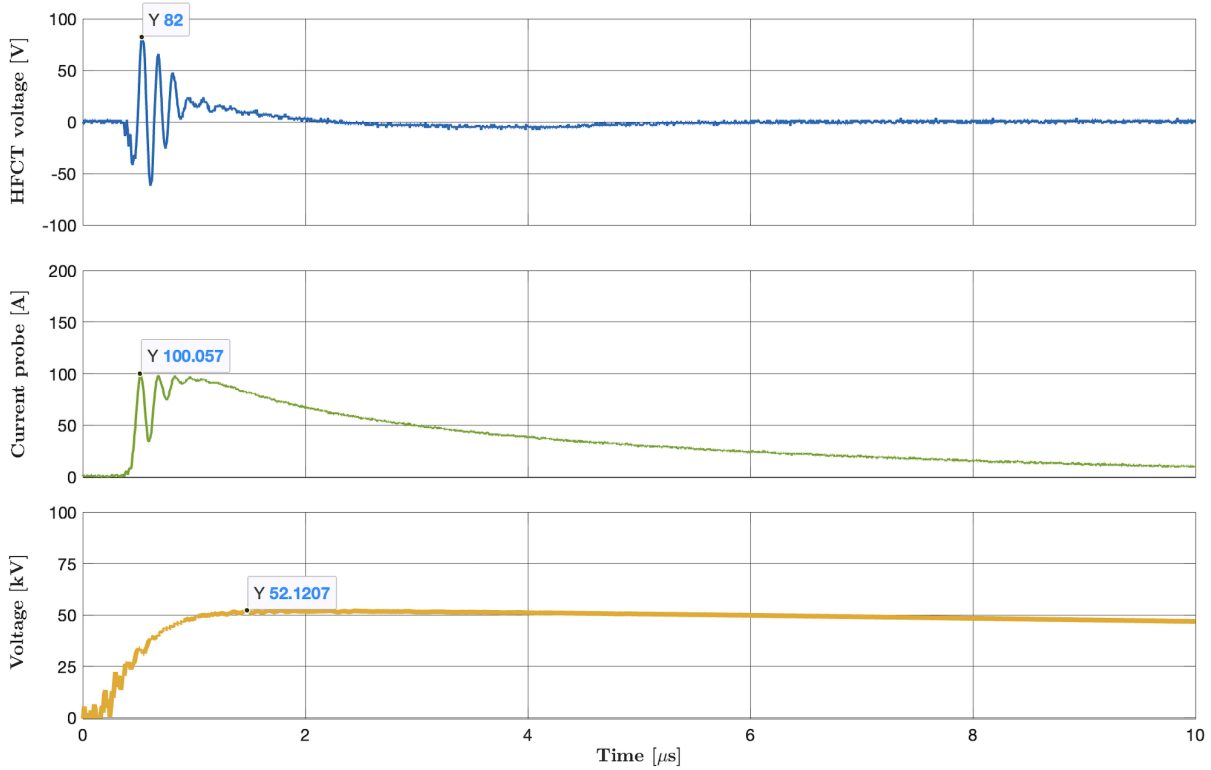

Figure 4.11: Scope images of HFCT output voltage, current measurement and the applied voltage for an 80 kV lightning impulse.

Starting with the scope image from the HFCT output voltage, it is evident that the oscillations from the initial spark still are present with a peak value of 82 V. But, more interestingly it is observed that the oscillations start to have a descending curvature from the peak value. It can also be observed that it drops below zero after 2 μs, before rising and stabilizing at zero at $\sim$ 6 μs.

The current probe measures a current amplitude of 100.1 A, but there are still some oscillations due to the initial spark from the impulse generator. After the oscillations, the current measurement drops inversely proportional down towards zero. The applied voltage was set to 80 kV but the voltage amplitude was found to be 52.1 kV. The resulting relationship between the applied and measured voltage is found to be 0.65.

4.3.3 160 kV - 200 A

Once again, the voltage and current are doubled from 80 kV - 100 A to 160 kV - 200 A. Two stages of the impulse generator had to be utilized and each stage had to be charged up to 80 kV. The resulting scope images of the HFCT output voltage, current measurement and measured voltage are presented in Figure 4.12.

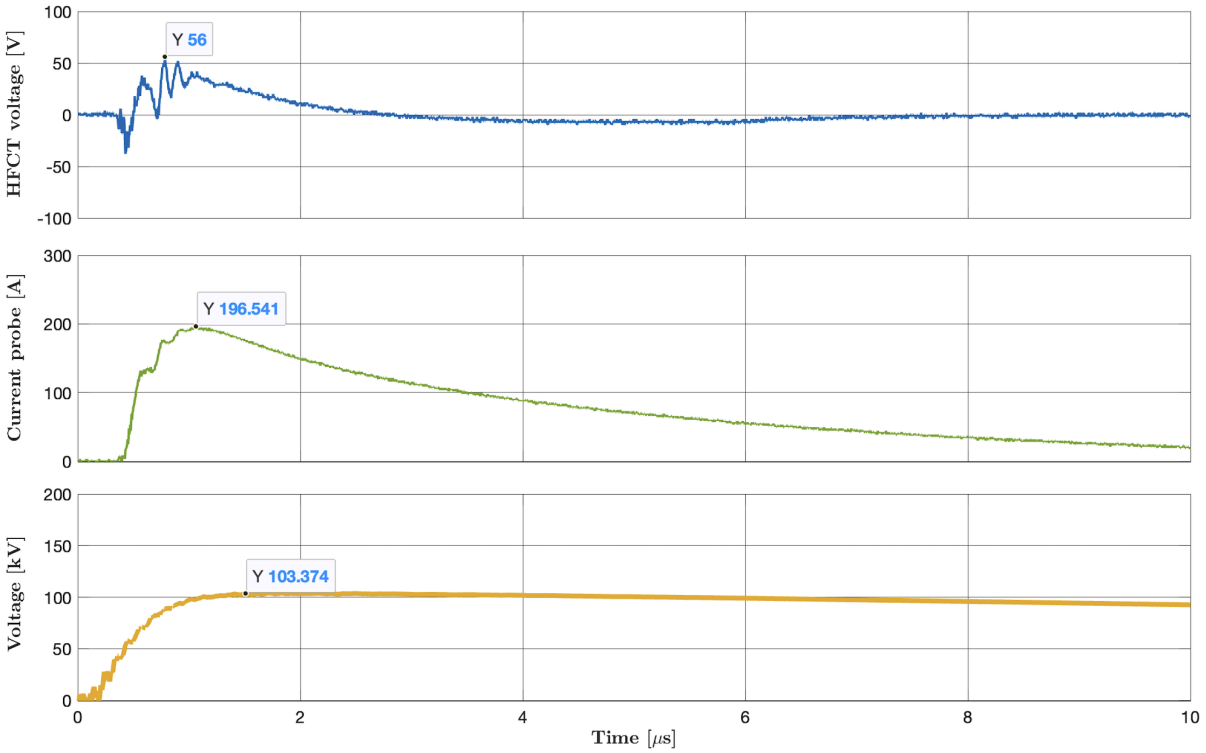

Figure 4.12: Scope images of HFCT output voltage, current measurement and the applied voltage for a 160 kV lightning impulse.

As is evident from the scope images, the HFCT voltage waveform is now more similar to the waveform of the current probe. It is still oscillating, but not nearly as much as during the previous 80 kV - 100 A lightning impulse. The amplitude of the HFCT output voltage is found to be 53 V which is in fact a decrease from the previous lightning impulse, however, this is assumed to mostly originate from the initial spark alone.

After reaching the voltage amplitude of 56 V, the voltage curve decreases inversely down and will face a polarity reversal. The HFCT voltage will contain this polarity reversal from approximately 3 μs to 8 μs, before stabilizing at zero voltage. The polarity reversal is small compared to the peak voltage, and thus should not pose any threat. This is beginning to correlate with the exponential impulse current theory explained in Section 2.4.1.

The current probe measured a peak current of 196.5 A, and the waveform of the current now contains even less of the oscillations that were present during the previously presented lighting impulse tests. The applied voltage was set to 160 kV but the measured voltage across the test object and resistor was found to have an amplitude of 103.4 kV. As a result, the relationship between the applied and measured voltage is found to be 0.65.

4.3.4 200 kV - 250 A

The last lightning impulse test performed was done with two fully charged stages of the impulse voltage test system, where each stage has the ability to charge to 100 kV. The resulting scope images from the 200 kV - 250 A lightning impulse of the voltage from the HFCT, current measurement and applied voltage are presented in Figure 4.13.

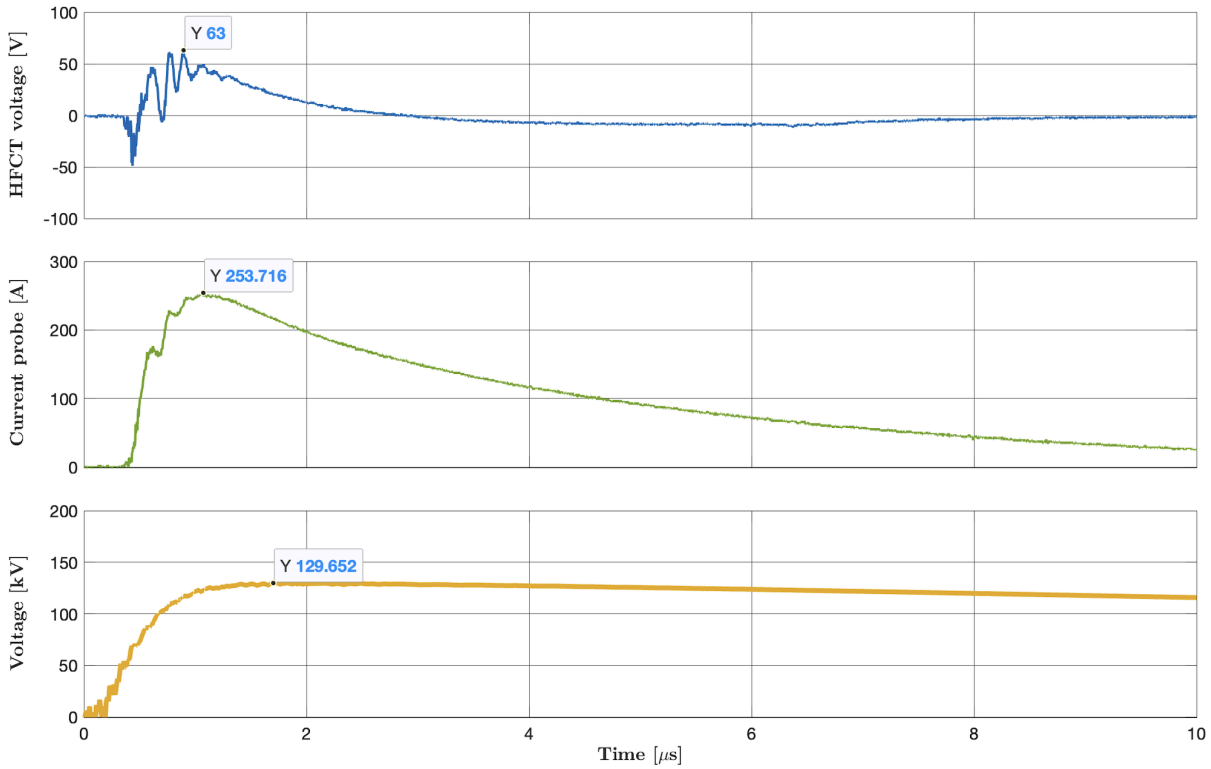

Figure 4.13: Scope images of HFCT output voltage, current measurement and the applied voltage for a 200 kV lightning impulse.

The waveform of the HFCT output voltage seems to have very similar characteristics with the previous lightning impulse at 160 kV, however, the amplitude has now increased to 63 V. The measured voltage amplitude is also lower than during the 80 kV impulse, which had a voltage amplitude of 82 V. The previous voltage amplitude of 82 V occurs earlier than the amplitude during this test, which indicates that it most likely origins from the initial spark of the impulse generator.

The current probe measured a current amplitude of 253.7 A through the test object, and the waveform is nearly without any of the previous oscillations caused by the initial spark. It is assumed that lightning impulses with a higher applied voltage amplitude will smooth out the HFCT output voltage in the same fashion as has been done for the current probe. A decomposition of the HFCT output voltage would most likely reveal that it contains two individual signals, where one is the oscillation due to the initial spark from the impulse generator and the other is the magnetic field from an exponential impulse current.

The applied voltage was set to 200 kV, however, the measured voltage across the test object and resistor was found to be 129.7 kV. This results in a relationship between the applied and measured voltage to be 0.65.

4.4 Magnetic field simulations

The purpose of performing the magnetic field simulations in COMSOL was to examine how simulated values compared to the values gathered from the 50 Hz AC current experiment. All simulations were performed in 3D with the previously explained configurations, outlined in Section 3.4. This section will begin by presenting the results from the simulations performed to validate the experimental setup. After that, it will present the results from the HFCT orientation and distance from cable simulations.

4.4.1 Validation of experimental setup

A line plot of the simulated magnetic flux density in COMSOL is presented in Figure 4.15. The conductor was set to carry a current of 1000 A. The measurements of the magnetic flux density are conducted at distances ranging from 0 to 150 mm as indicated through the red cut line in Figure 4.14, with a measurement interval of 5 mm.

By closely inspecting the cut line shown in Figure 4.14, it can be seen that it does not extend all the way to the cable conductor. This is done deliberately because considerations to the thickness of the cable insulation have been thought of. This is in line with how the experimental tests for magnetic flux density measurements were conducted.

The resulting line plot presented in Figure 4.15 reveals that the magnetic flux density starts at roughly 10 mT before descending inversely proportionally towards zero, in a similar fashion as the experimentally measured magnetic flux density. In the following section, further analysis of the simulation will be discussed through a combined comparison of the simulated, experimentally measured and analytically calculated magnetic flux density.

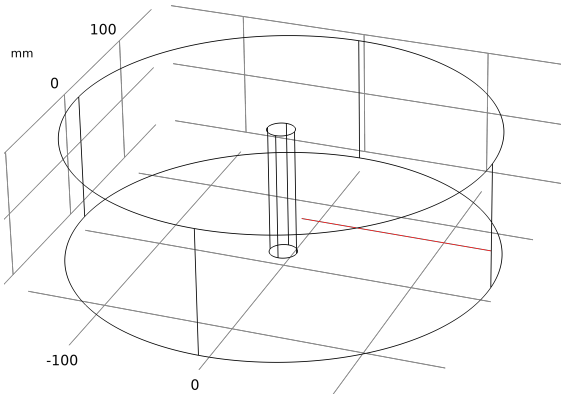

Figure 4.14: Cut line for the obtained magnetic flux density indicated in red on the right side of the conductor.

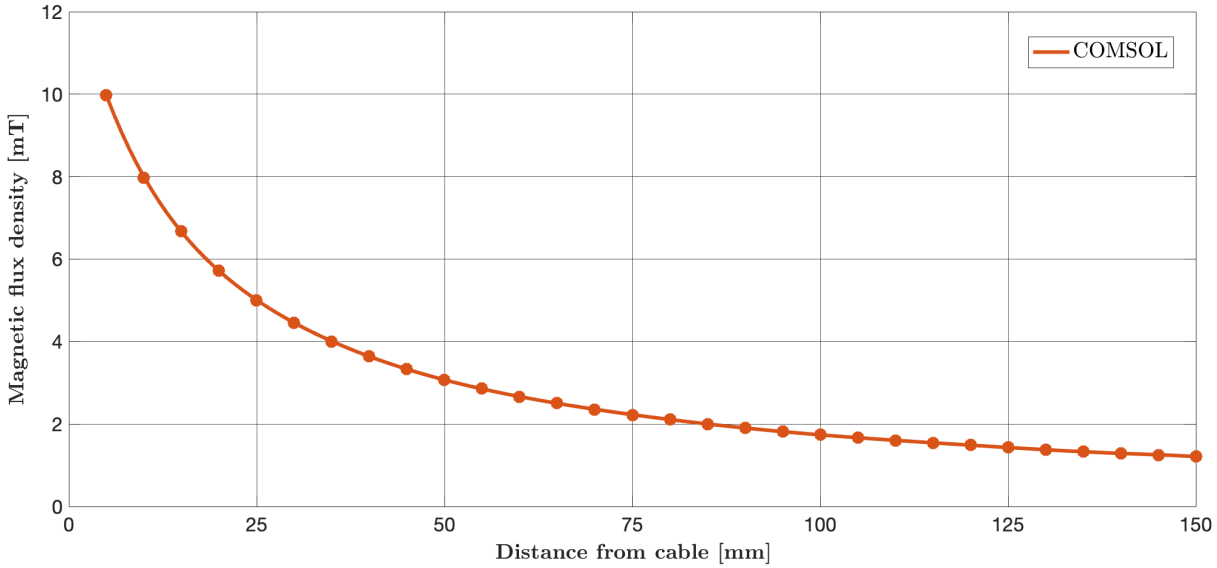

Figure 4.15: The magnetic flux density obtained from magnetic field simulations done in COMSOL. The magnetic flux density was evaluated through the cut line shown in Figure 4.14.

4.4.2 HFCT orientation and distance from cable

Based on the results gathered from the initial 50 Hz AC current experiments, it was decided to only pursue the simulations with the best and worst HFCT orientation, orientations 1 and 2. Line plots of the simulated HFCT output voltage as a function of distance from the cable are presented in Figure 4.16.

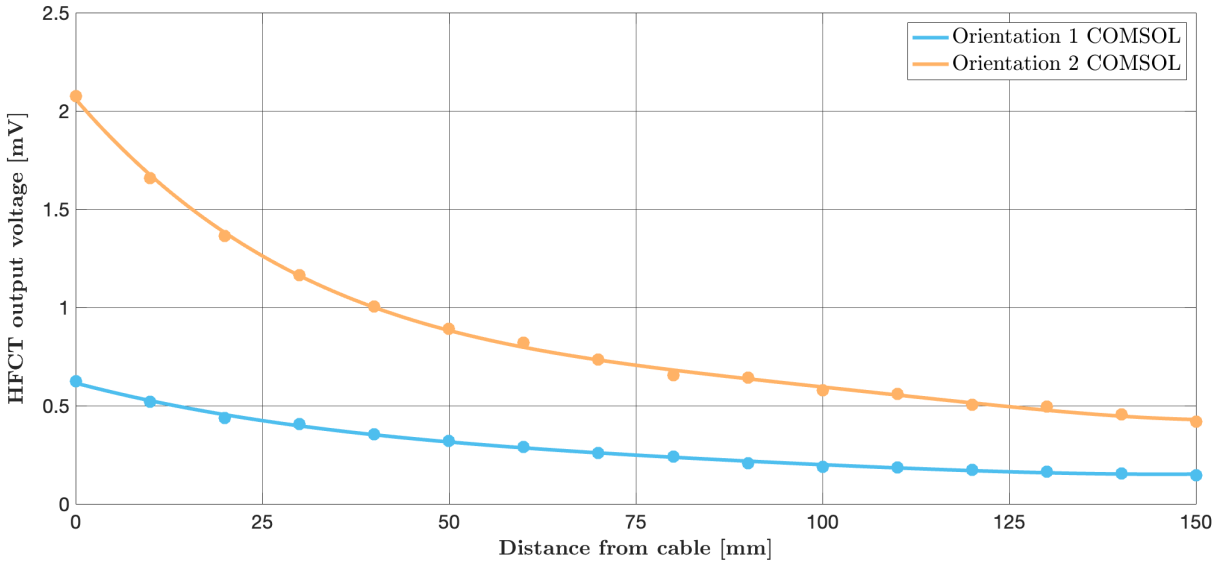

Figure 4.16: Line plots of the simulated HFCT output voltage for orientation 1 and 2 as a function of distance. A parametric sweep was performed with a measurement interval of 10 mm.

The observation obtained from the line plots in Figure 4.16 reveals that HFCT orientation 2 exhibits a higher output voltage compared to orientation 1. This conforms with the previously presented results of the measured HFCT output voltage during the 50 Hz AC current experiment. Further analysis will be performed in the discussion section, where the simulated output voltages will be compared to the measured output voltage during the 50 Hz AC current experiments.

To gain a deeper insight as to why orientation 1 is superior compared to orientation 2, a graphical illustration of the magnetic field and magnetic flux density will be presented. Starting with orientation 1, Figure 4.17 presents the resulting magnetic field lines and flux density within the ferrite core.

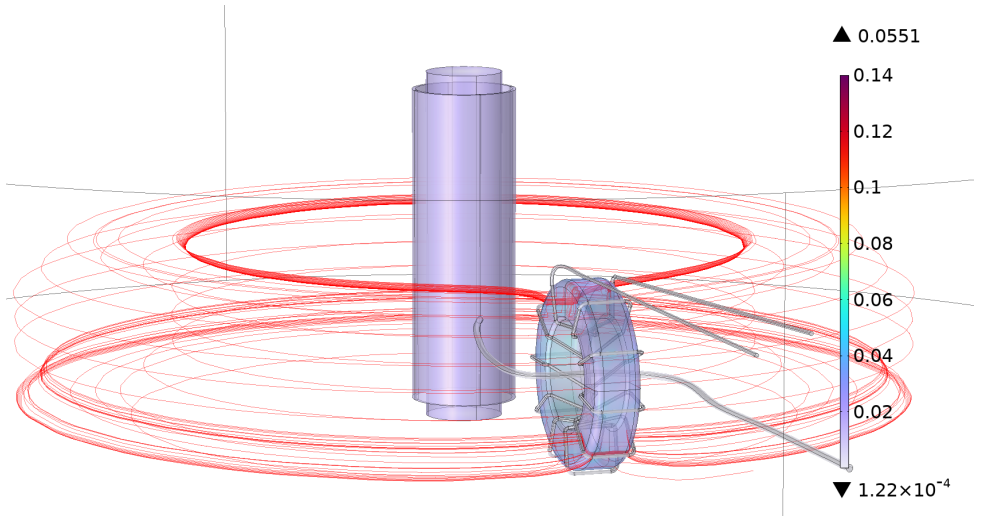

Figure 4.17: The simulated magnetic field lines and the magnetic flux density in Tesla when HFCT is in orientation 1.

Figure 4.17 visually demonstrates the attraction of the magnetic field to the ferrite core and the resulting magnetic flux density within the core. The attraction of the magnetic field to the ferrite core is due to the high permeability it possesses. The magnetic flux that accumulates in the core does not have much room to move, with regards to the magnetic field direction, to generate an output voltage. A volume average of the magnetic flux density within the core was performed and was found to be 11.13 mT.

Moving onto orientation 2, Figure 4.18 presents the magnetic field lines and flux density within the ferrite core. It is worth noting that the colour scale for the magnetic flux density remained the same for both illustrations.

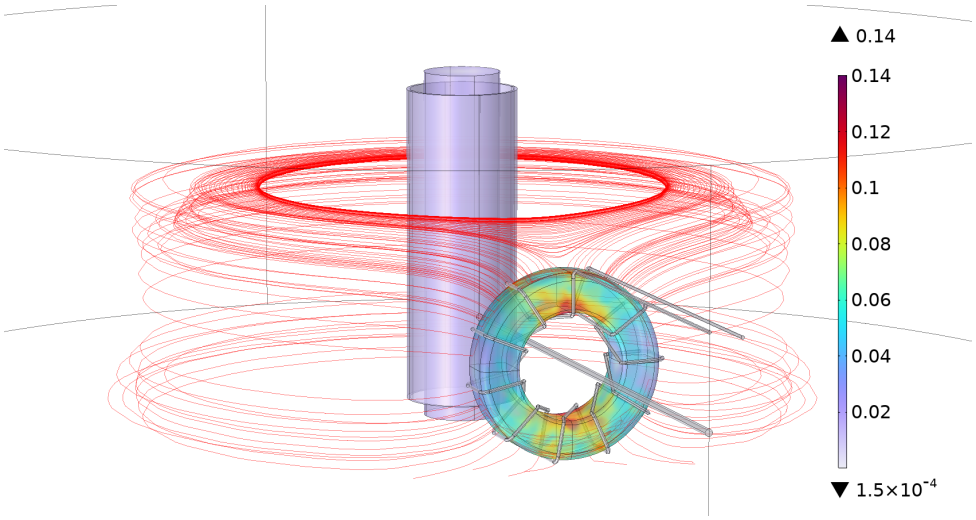

Figure 4.18: The simulated magnetic field lines and the magnetic flux density in Tesla when HFCT is in orientation 2.

In Figure 4.18, a significant concentration of magnetic flux density within the ferrite core can be observed, especially in the upper and lower regions of the core. The magnetic flux in the core now has more room, where it flows from one side to the other, and will, as a result, generate a higher output voltage. This is a result of a higher magnetic flux density within the core. The volume average magnetic flux density within the ferrite core was found to be 30.34 mT, which is nearly three times higher compared to HFCT orientations 1. This will again have a direct influence on the core saturation, output voltage amplitude and waveform characteristics.

5 Discussion

Throughout this section, the results gathered from the experiments, simulations and analytical calculations will be compared, analyzed and discussed. This section will begin by comparing the result from the magnetic field simulation, experiments and analytical calculation for the validation of the experimental setup. Following, a similar comparison will be done for the HFCT orientation and distance from the cable. Next, a discussion of the HFCT sensitivity to breaker activity and an evaluation of the effect of lightning impulses. Lastly, a general discussion will be given to summarize the remaining possible errors.

5.1 Validation of the experimental setup

A comparison of the values obtained from the experiments, COMSOL and analytical calculations is presented in Figure 5.1. Commonly for all three techniques, the current through the cable was kept at 1000 A while the magnetic flux density was measured in intervals of 5 mm.

To obtain the values for the analytical calculations, Equation 2.11 from Section 2.5.2 has been used with consideration to the cable insulation thickness. A complete table of all the experimentally, simulated and analytically obtained magnetic flux density values can be found in Appendix D.

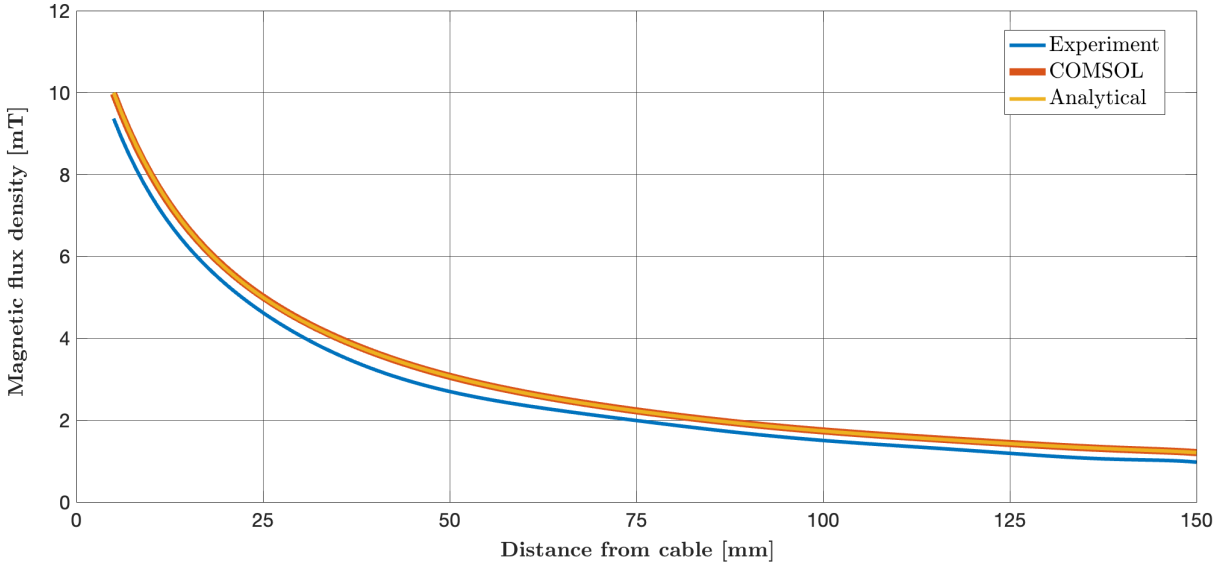

Figure 5.1: A comparison of the measured, simulated and calculated magnetic flux density at distances from 5 to 150 mm away from cable. The applied current was set to 1000 A and the measurement interval was 5 mm.

As can be observed from Figure 5.1, the values obtained from COMSOL simulations and analytical calculations remained identical while the values obtained during the experiment has a small deviation. This can be caused by inaccurate distance measurements during the experiment. Another possible error may be that the cable in the laboratory was bent and looped causing an opposing magnetic field which may reduce the measured magnetic flux density. For the simulations and the analytical calculations, the cable is assumed straight and infinitely long. In addition, the ground plane present during the experiments where not considered in the simulations or the calculations. This can also have been part of the reason for the deviations.

Even though the measured magnetic flux density from the experiments deviated from the simulated and analytically obtained magnetic flux density, the deviation remained constant. This indicates that the experimental results were credible, and resulted in the continuation of developing the models in COMSOL to include the copper mesh and High-Frequency Current Transformer.

5.2 The effect of HFCT orientation and distance from cable

Based on the previously presented results, a comparison of the HFCT output voltage as a function of distance between simulations and experiments is presented in Figure 5.2. It was chosen to only pursue with the best orientation, 1, and the worst orientation, 2, in the simulation. A complete table of all the values that makes this line plot can be found in Appendix E.

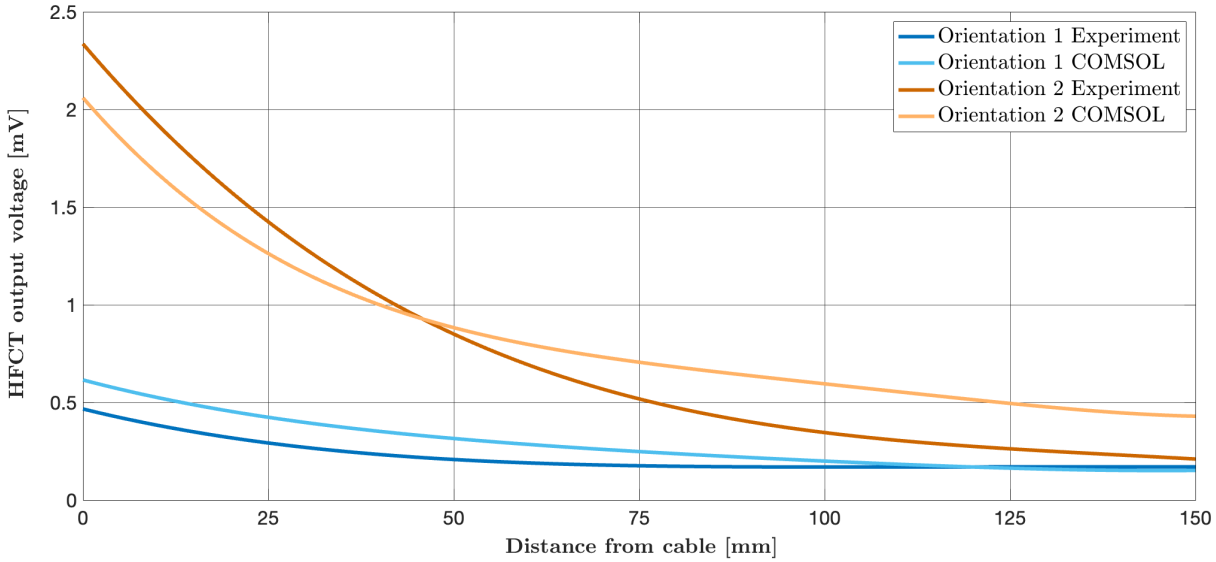

Figure 5.2: A comparison of HFCT output voltage between the simulations and experiments.

As can be observed in the comparison, the simulated and experimentally obtained generally aligns, however, there are some deviations. Starting with orientation 1, the difference between the experimentally obtained and simulated output voltage is found to be small. The simulated values reveal an initially higher output voltage which intersects the experimentally obtained voltage at $\sim$ 120 mm. This is assumed to occur due to the fact that the experimentally obtained HFCT output voltage remained constant after 75 mm due to the external noise present during the experiments. The magnetic field simulations performed in COMSOL do not have to deal with external noise, and can therefore simulate the HFCT output voltage to zero.

For orientation 2, the difference between the experimentally obtained and simulated output voltage is larger. To begin with, the simulated output voltage reveals an initially lower output voltage before intersecting the experimentally obtained voltage at 45 mm. After the intersection, the deviation between the output voltage comparison increases. It remained unsure as to why the deviations between the measured and simulated output voltages were greater for orientation 2 than orientation 1, however, possible reasons will be discussed.

In conclusion, the magnetic field simulations and the experimentally obtained output voltages generally aligned, however, there are some deviations. There are several possible reasons for the deviations present in the comparison, but the three most important reasons are HFCT modelling, the material composition of the ferrite core and a low degree of model meshing.

Starting with HFCT modelling, the HFCT was modelled according to manual measurements taken of the ferrite core and windings, however, it does not include the outer casing as shown in Figure 5.3. The outer casing was not modelled as it is made out of aluminium, a paramagnetic material which does not have any contribution to the magnetic field. It is however assumed that a higher degree of HFCT modelling will yield better results, partly due to the winding configurations. The HFCT should be constructed in a Computer-Aided Design (CAD) software, such as SolidWorks, and then be imported into COMSOL.

Figure 5.3: The modelled High-Frequency Current Transformer in COMSOL and the Tekbox TBCP1-250 current transformer.

The next uncertainty is also related to the HFCT, but now the material composition of the ferrite core. In the manual for the Tekbox TBCP1-250, it is specified that the HFCT offers a usable bandwidth ranging from 10 kHz and all the way up to 250 MHz. Given the high-frequency bandwidth it offers in combination with the theory on ferrite core explained in Section 2.3, it is assumed that the ferrite core is made out of Nickel-Zinc (NiZn). NiZn ferrites are typically used for Radio-frequency (RF) transformers and pulse power devices where switching occurs in the nanoseconds region. NiZn ferrite cores are characterized by having a permeability below 2500, and thus the permeability was chosen to be 2000 in the simulations.

However, as demonstrated by the Tekbox TBCP1-250 transfer impedance presented in Figure 5.4, the permeability of a ferromagnetic material is frequency dependent. As a result, the frequency dependency should be modelled, which will become crucial when performing magnetic field simulations for fast-acting transient currents. In COMSOL it is possible to manually configure an effective hysteresis curve B(H), which the manufacturer of the HFCT may be able to provide upon request.

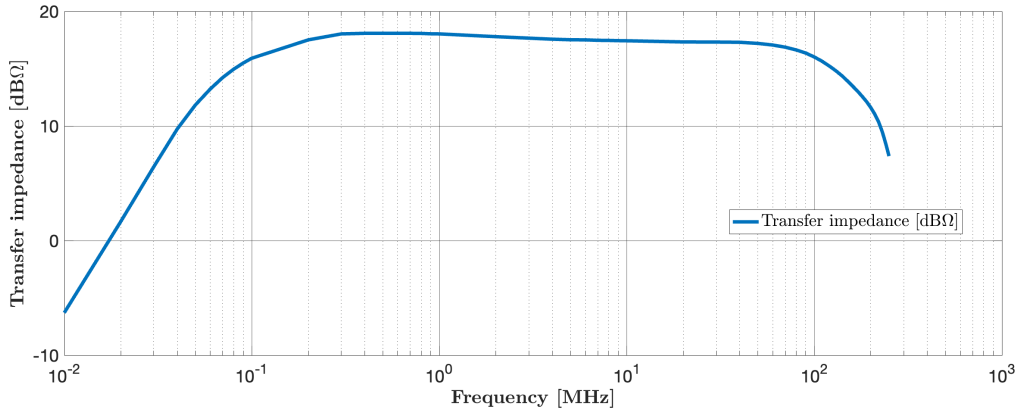

Figure 5.4: The frequency dependent transfer impedance for the Tekbox TBCP1-250 [39].

The last inaccuracy that will be discussed is the element meshing of the COMSOL model. The model meshing was performed through the physics-controlled option at an element size of finer, giving a decent degree of meshing. However, an even finer and more optimal meshing can be done manually, but it will come at the cost of computational power and time required. It was experienced that the requirements for computational power and time were quite high already, and a finer meshing will demand even more. If the HFCT is subjected to be modelled with a higher degree of accuracy, it will increase the mesh elements even further.

5.3 Sensitivity to breaker activity

The main purpose of the switching transient experiment was to evaluate how a re-strike, and a following fast-acting transient current, would affect the inductive partial discharge sensor. Even though the re-strike attempts remained unsuccessful, interesting results due to circuit breaker activity were discovered. The previously presented scope image of HFCT output voltage in Figure 4.5, revealed that a peak voltage of 65.6 V was detected during the initiation of SC current through the CB, and the peak voltage amplitude can be higher due to the low sampling-rate of the used oscilloscope. There are some concerns regarding the high magnitude of this voltage which can potentially cause damage to sensitive partial discharge measurement systems.

It is especially relevant, as a cable termination will be in close proximity to circuit breakers inside a substation. In order to succeed with the SmartACT project objective that the sensor shall have a longer lifetime than the cable termination itself, then safety measures have to be implemented. These measures are crucial to enable proper safety precautions to prevent potential damaging voltage spikes to the PD measurement system.

The safety measures have to involve sufficient dampening of the HFCT output signals, but more importantly, it should not negatively affect the sensitivity of the partial discharge interpretation. Throughout this thesis, the use of attenuators, end-terminations and gas discharge tubes have proven to be viable options. Further protection can be done through the use of a diode configuration, however, this option has not been explored in this master thesis.

Another important aspect is that the tests were carried out with an applied voltage of 13.8 kV. At 420 kV, the HFCT output voltage due to circuit breaker activity may become increasingly higher, due to the significantly higher applied voltage and current. This is something that should be further investigated on a full-scale cable termination.

5.4 The effect of lightning impulses

The previously presented results in Section 4.3 indicated that the HFCT is affected by the lightning impulse, however, the output voltage seems to be made up of two different components. For comparison, the HFCT output voltages for the 40 kV and 200 kV applied voltage tests are presented in Figure 5.5.

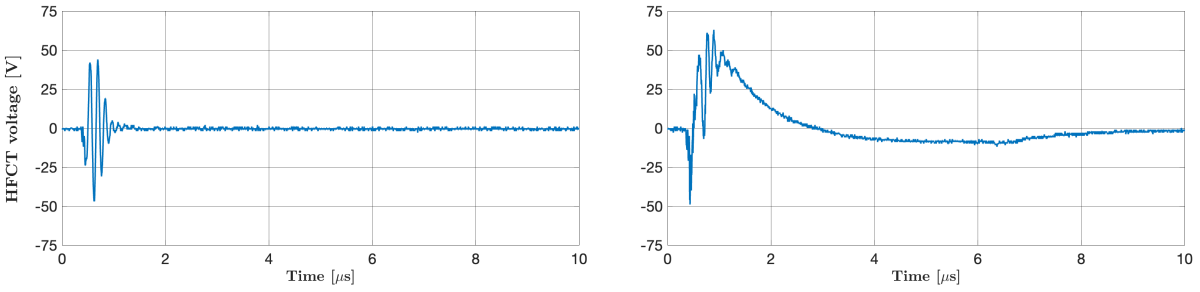

(a) 40 kV - 50 A **(b)** 200 kV - 250 A

Figure 5.5: Comparison of the HFCT output voltage when then applied was set at 40 kV and 200 kV, resulting in 50 A and 250 A respectively.

From the comparison, it becomes evident that the 40 kV - 50 A test mainly results in an oscillation output voltage. Meanwhile, for the 200 kV - 250 A test, the oscillations are more overshadowed by the lightning impulse current than the oscillations and as a result, have more of a curvature of an exponential impulse current. To further investigate this, a Fast Fourier Transformation (FFT) of both signals has been performed which is presented in Figure 5.6.

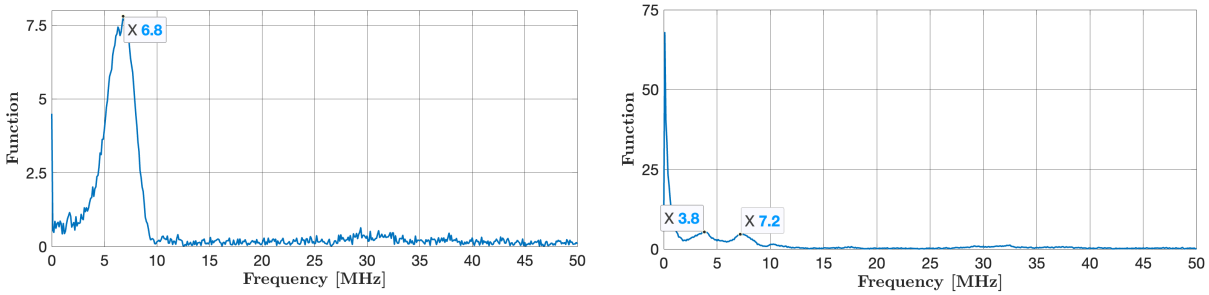

(a) FFT 40 kV - 50 A

(b) FFT 200 kV - 250 A

Figure 5.6: Comparison of the Fast-Fourier Transform when then applied was set at 40 kV and 200 kV, resulting in 50 A and 250 A respectively.

The FFTs presented in Figure 5.6, reveal that the oscillating component of the 40 kV - 50 A has a frequency of 6.8 MHz. For the 200 kV - 250 A impulse, the FFT shows two frequencies 3.8 and 7.2 MHz. This is significantly faster than the front-time frequency of the lightning impulse, which is estimated in Equation 5.1

$$f_{T_1} = \frac{1}{3 \cdot \mathrm{T}_1} = \frac{1}{3 \cdot 1 \cdot 10^{-6}\ \mathrm{s}} = 333.33\ \mathrm{kHz} \tag{5.1}$$

Based on the FFTs and the frequency of the lightning impulse front-time, it is assumed that the oscillations originate from the Marx generator's initial spark and thus will not be the same for a full-size termination situated inside a substation. However, there should still be a concern if the lightning strike occurs in close proximity to the substation, as it will emit similar high-frequency electromagnetic pulses which will produce a significantly higher HFCT output voltage.

The tested voltage and current levels are significantly lower than what is to be expected from an actual lightning event. As a result, the output voltage from the HFCT is expected to be a lot higher during a real lightning event. Typical lightning currents are in the range of thousands of amperes, and will thus generate a remarkably higher magnetic field and thus higher HFCT output voltage. The magnitude of the HFCT output voltage is dependent on both the orientation and distance away from the cable, however, it is suspected that it may be in the range of several hundreds of volts during a real lightning event.

Further experiments with increasing lightning impulse voltages and currents can be conducted, such that an estimation factor can be established. The estimation factor can be drawn out from a statistical study of HFCT output voltage with an increase in applied lighting impulse voltage and current. Using this factor, it should be possible to estimate the worst-case scenario for the HFCT output voltage for an authentic lightning event.

5.5 General

This thesis has proven important aspects regarding how the inductive partial discharge sensor should be positioned inside the oil-filled outdoor cable termination. It has been discovered that when positioned in orientation 1, it is significantly less affected by the emitted magnetic field from a cable compared to other orientations. The distance also plays an important role, and the results indicate that the HFCT should be positioned as far away from the cable as possible. However, further testing on a full-scale termination will be necessary as the result can be different due to the higher current magnitudes present during normal operation and fault situations.

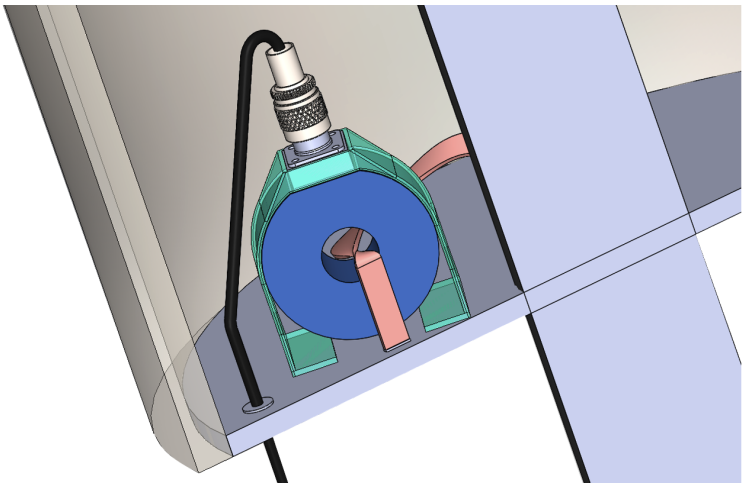

Figure 5.7: Illustration of the HFCT installed inside a cable termination in orientation 1. The HFCT is positioned in a 3D-printed stand to secure its position and the copper mesh is threaded through it.

Saturation of the ferrite core has not been proven to be a concern if the HFCT is positioned sufficiently far away from the cable and in the correct orientation. The main concern with saturation is not during fast-acting transients, but during high stationary load currents. Experiments conducted in HFCT orientation 1 were with an applied current of 1000 A, but in the power grid, it can be several thousands of amperes. As a result, further testing with a higher applied current should be performed to evaluate the risk of core saturation.

The magnetic field simulations have only been performed on a 12 kV PEX insulated cable, necessitating the need to create a model for a 420 kV cable. The model can easily be scaled up to include 420 kV cable. However, even though the obtained simulation results generally conformed to the experimentally found, a higher simulation accuracy should be obtained before scaling it up. Once higher simulation accuracy is obtained through the previously mentioned model modifications, then a scaled-up version can be made to perform a variety of fault scenarios.

During the 50 Hz AC current experiments, a weakness with the applied current was present as it had to be manually adjusted through a variable autotransformer (variac). This resulted in the applied current not being precisely 1000 A as in the magnetic field simulations performed. Even though it was difficult to apply the current, it always remained within the range of 1000 ± 20 A.

6 Conclusion

This thesis has investigated how transient magnetic fields will affect the inductive partial discharge sensor and the conclusion drawn can be summarized as follows.

- The orientation of the High-Frequency Current Transformer (HFCT) has been found to significantly influence how much the sensor is affected by the magnetic field. Experimental evaluations of three sensor orientations revealed that orientation 1, standing perpendicular to the cable, is the least affected by the emitted magnetic field. In contrast, orientation 2, standing parallel to the cable, is the most influenced and its core will even go into saturation when positioned in close proximity to the cable.
- The distance between the cable and HFCT was also discovered to be an important factor in terms of HFCT output voltage. Through experiments, it has been revealed that the HFCT output voltage decreases with an increase in distance. The rate of decrease indicates to follow the same rate as the magnetic flux density, which decreases inversely proportionally at a rate of 1/r.
- Magnetic field simulations to evaluate HFCT orientation and distance were successfully performed in COMSOL. The simulation results generally aligned and conformed with the experimental findings, although some deviations were observed. The deviations are assumed to originate mainly due to three reasons: inaccurate HFCT modelling, low degree of meshing and unknown material composition of the ferrite core.
- Experiments with short circuit current with and without decaying DC component, current interruption and current re-strike were performed. The current re-strike experiment was expected to have the most influence on the inductive sensor, however, it remained unsuccessful. Interestingly, the results obtained from the remaining tests revealed that the main concern does not lie with neither the short circuit current nor the current interruption, but rather the activity from the circuit breaker in the laboratory. This should be further investigated at higher voltage levels, as a cable termination typically will be placed inside a substation and is therefore in the vicinity of circuit breakers and switches.
- Lightning impulse tests were conducted with applied voltages ranging from 40 to 200 kV, resulting in a peak current of 250 A. Relatively high voltage oscillations were present at the initial lightning impulse tests performed, which were assumed to originate from the Marx generator spark gap. For the lightning impulse with an applied voltage of 200 kV, the shape of an exponential impulse current shape seems to overshadow the oscillations as the waveform of an exponential impulse current is present. Similar to during the switching transient experiment, the HFCT output voltage was found to be quite high and will also increase with an increase in applied impulse voltage and current.

The culmination of results obtained throughout this thesis has proven that the emitted transient magnetic field from a cable will affect the inductive sensor and provides the following recommendations. Firstly, it lays an important foundation in the selection of HFCT orientation and distance from the cable. For the sensor to be minimally impacted by the magnetic field, then it should be positioned in orientation 1, perpendicular with regards to the cable, and as far away as possible from the cable, given the limitations imposed by the cable termination itself.

Secondly, high output voltage amplitudes due to breaker activity and lightning impulses will occur. The main concern with these high voltage amplitudes is not directed to the HFCT, but rather the sensitive partial discharge measuring system that it is connected to. As a result, it acts as a foundation for investigating an overvoltage protection scheme to ensure the longevity required of the sensor.

7 Further work

Based on the experimental results gathered from both this thesis and the specialisation project [14] completed in the fall of 2022, suggestions for further work are.

- Further development of the 3D magnetic field models in COMSOL should be focused in order to increase simulation accuracy. In particular, a more detailed modelling of the High-Frequency Current Transformer (HFCT) should be done through a CAD software, such as SolidWorks. Also, the HFCT core material properties such as permeability as a function of frequency should be implemented in the COMSOL model. If the new improved model shows an increase in simulation accuracy, then the magnetic field models can be scaled up to a 420 kV mode, and a variety of fault scenarios, such as switching transients and lightning impulses can be conducted.
- Protection against high HFCT output voltage amplitudes that can harm sensitive partial discharge measuring systems. This thesis has revealed that high output voltages can, and will, occur due to breaker activity and lightning impulses, therefore necessitating the need to create an overvoltage protection scheme. The overvoltage protection may consist of attenuators, gas discharge tubes, end-terminations or diodes. It is recommended to perform an experimental study to find the optimal protection system, which shall prevent or dampen the high voltage amplitudes while maintaining the sensitivity and performance of the sensor to detect partial discharges.
- An experimental study to evaluate the development of defects over time. Partial discharge within a cable termination leads to slow degradation of the insulation, but there are no guidelines available today that define when a component should be replaced. As a result, measures to predict the complete breakdown should be considered through experiments, where factors such as partial discharge magnitude and rate over time are important.
- More testing on a full-scale 420 kV cable termination to ensure the longevity and sensitivity required of the sensor. The testing should include both the electrical transients covered in this thesis and partial discharge detection with the inductive sensor. The main concern is how large the voltage amplitude due to breaker activity and lightning impulses can be and if the HFCT will face saturation at a higher applied current. For PD detection, previous work in the specialisation project was done for a 12 kV termination in air. However, the behaviour of PD in an oil-filled termination should be further examined.

Bibliography

[1] E. Ildstad, 'Compendium: High Voltage Equipment - Cable', 2022.

[2] Brugg Cables, 'High Voltage Cable Accessories', 2022. [Online]. Available: https://bruggcablesshop.nuboserv.com/webdocs/BKAG_HVCA-Brochure_en.pdf.

[3] L. Zhong, Y. Xu, G. Chen, A. Davies, Z. Richardson and S. Swingler, 'Use of capacitive couplers for partial discharge measurements in power cables and joints', in *ICSD'01. Proceedings of the 20001 IEEE 7th International Conference on Solid Dielectrics (Cat. No.01CH37117)*, 2001, pp. 412–415.

[4] D. Denissov, W. Köhler, S. Hoek, S. Tenbohlen and T. Klein, 'On-line partial discharge diagnostics for cable terminations', Jan. 2007.

[5] Statnett, avdeling Feilanalyse, Personal Communication, 2022.

[6] F. Álvarez, F. Garnacho, J. Ortego and M. Sánchez-Urán, 'Application of HFCT and UHF Sensors in On-Line Partial Discharge Measurements for Insulation Diagnosis of High Voltage Equipment', *Sensors (Basel, Switzerland)*, vol. 15, pp. 7360–87, Apr. 2015.

[7] M. Fritsch and M. Wolter, 'High-Frequency Current Transformer Design and Construction Guide', *IEEE Transactions on Instrumentation and Measurement*, vol. 71, 2022.

[8] A. Krontiris and G. Balzer, 'Condition assessment of power system equipment the impact of ageing and deterioration', Jan. 2008.

[9] E. Ildstad, 'TET4585 - Part 1 Condition Assessment, Seminar 1 General Introduction', 2022.

[10] E. Ildstad, 'TET4585 - Part 1 Condition Assessment, Seminar 2 Destructive tests and laboratory sample analysis', 2022.

[11] Forskningsrådet. 'Smart On-Line Health Assessment of Cable Terminations'. (2021), [Online]. Available: https://prosjektbanken.forskningsradet.no/project/FORISS/318007 (visited on 23rd Jan. 2023).

[12] SINTEF. 'SmartACT - Smart On-Line Health Assesment of Cable Terminations'. (2021), [Online]. Available: https://www.sintef.no/prosjekter/2021/smartact-smart-on-line-health-assessment-of-cable-terminations (visited on 23rd Jan. 2023).

[13] Statnett. 'Trådløse sensorer skal overvåke tilstanden til kabeltermineringer'. (2021), [Online]. Available: https://www.statnett.no/om-statnett/innovasjon-og-teknologiutvikling/vare-sentrale-prosjekter/smartact/ (visited on 23rd Jan. 2023).

[14] B. H. Turi, 'On-line Condition Assessment of 420 kV Terminations – design and development of partial discharge sensors, Specialisation project in TET4510', Dec. 2022.

[15] E. Ildstad, 'TET4160 - Insulating Materials for High Voltage Applications', 2021.

[16] A. Küchler, *High Voltage Engineering - Fundamentals, Technology and Applications*. 2017.

[17] NEK, 'IEC 60270 - High-voltage test techniques, Partial discharge measurements', 2015.

[18] L. Lundgaard, 'Partial Discharges - General Description', 2008.

[19] S. Hvidsten, 'Power cables - Partial discharge measurements',

[20] Omicron, 'What is Partial Discharge?', 2020.

[21] C.-H. Lee, L. Yu-Chih, M.-Y. Chiu, H. Chih-Hsien, S.-S. Yen and C. Haeng, 'Recognition of partial discharge defects in cable terminations', in *2008 International Conference on Condition Monitoring and Diagnosis*, 2008, pp. 1242–1245.

[22] Y. Mecheri and S. Bouazabia, 'Effect of conductive contaminants on the electrical behavior of ehv xlpe cable insulation', in *2016 International Conference on Electrical Sciences and Technologies in Maghreb (CISTEM)*, 2016.

[23] K. Schon, *High Voltage Measurement Techniques - Fundamentals, Measuring Instruments, and Measuring Methods*. 2019.

[24] J. Ardila-Rey, M. Rojas-Moreno, J. Martínez-Tarifa and G. Robles, 'Inductive sensor performance in partial discharges and noise separation by means of spectral power ratios', *Sensors (Basel, Switzerland)*, vol. 14, pp. 3408–27, Feb. 2014.

[25] C. Zachariades, R. Shuttleworth, R. Giussani and R. MacKinlay, 'Optimization of a High-Frequency Current Transformer Sensor for Partial Discharge Detection Using Finite-Element Analysis', *IEEE Sensors Journal*, vol. 16, no. 20, pp. 7526–7533, 2016.

[26] J. V. Klüss, A.-P. Elg and C. Wingqvist, 'High-Frequency Current Transformer Design and Implementation Considerations for Wideband Partial Discharge Applications', *IEEE Transactions on Instrumentation and Measurement*, vol. 70, 2021.

[27] M. Fritsch and M. Wolter, 'Determination of the Optimal Air Gap of an HFCT', in *2023 IEEE Power & Energy Society Innovative Smart Grid Technologies Conference (ISGT)*, 2023.

[28] Elforsk, 'Cable System Transient Study : Vindforsk V-110. Experiments with switching transients and their mitigation in a windpower collection grid scale model', 2009.

[29] M. Sack, J. Ruf, D. Herzog and G. Müller, 'Modelling of a Resonant Charging Circuit for a Solid-State Marx Generator', *Applied Sciences*, vol. 12, no. 23, 2022.

[30] NEK, 'IEC 62067 - Power cables with extruded insulation and their accessories for rated voltages above 150 kV (Um = 170 kV) up to 500 kV (Um = 550 kV) – Test methods and requirements', 2022.

[31] NEK, 'IEC 60060 - High-voltage test techniques – Part 1: General definitions and test requirements', 2010.

[32] K. Niayesh and M. Runde, *Power Switching Components - Theory, Applications and Future Trends*. 2017.

[33] J. Zaborszky and J. W. Rittenhouse, 'Fundamental aspects of some switching overvoltages on power systems', *Transactions of the American Institute of Electrical Engineers. Part III: Power Apparatus and Systems*, vol. 81, no. 3, pp. 822–830, 1962.

[34] J. M. D. Coey, *Magnetism and Magnetic Materials*. Cambridge University Press, 2010.

[35] J. Skaar, 'Kompendium: Elektromagnetisme', 2017.

[36] T. Østrem, 'Kompendium: Kraftelektronikk og elektriske maskiner', 2019.

[37] B. A. Siddiqui, P. Pakonen and P. Verho, 'Novel inductive sensor solutions for on-line partial discharge and power quality monitoring', *IEEE Transactions on Dielectrics and Electrical Insulation*, vol. 24, no. 1, pp. 209–216, 2017.

[38] COMSOL, 'AC/DC Module User´s Guide', 2018. [Online]. Available: https://doc.comsol.com/5.4/doc/com.comsol.help.acdc/ACDCModuleUsersGuide.pdf.

[39] T. D. Solutions. 'TBCP1-250 RF CURRENT MONITORING PROBE'. (2023), [Online]. Available: https://www.tekbox.com/product/tbcp-rf-current-monitoring-probes/ (visited on 27th Feb. 2023).

Appendices

A List of equipment

A.1 50 Hz current experiment

Table A.1: Equipment used for the test object, laboratory and measurement setup during the 50 Hz AC current experiments.

Category	Equipment
Laboratory setup	Variable autotransformer
	Split-core current transformer
	Fluke i1010 current clamp meter
	AMPROBE AC50A current clamp meter
Test object	1 x 240 mm^2 Cu cable
	Tekbox TBCP1-250 HFCT
	Copper mesh
	Aluminium base plate
Measurement setup	FLIR C3 Thermal camera
	GM08 Gaussmeter
	Keysight DSOX2014A Oscilloscope
	Coaxial cable

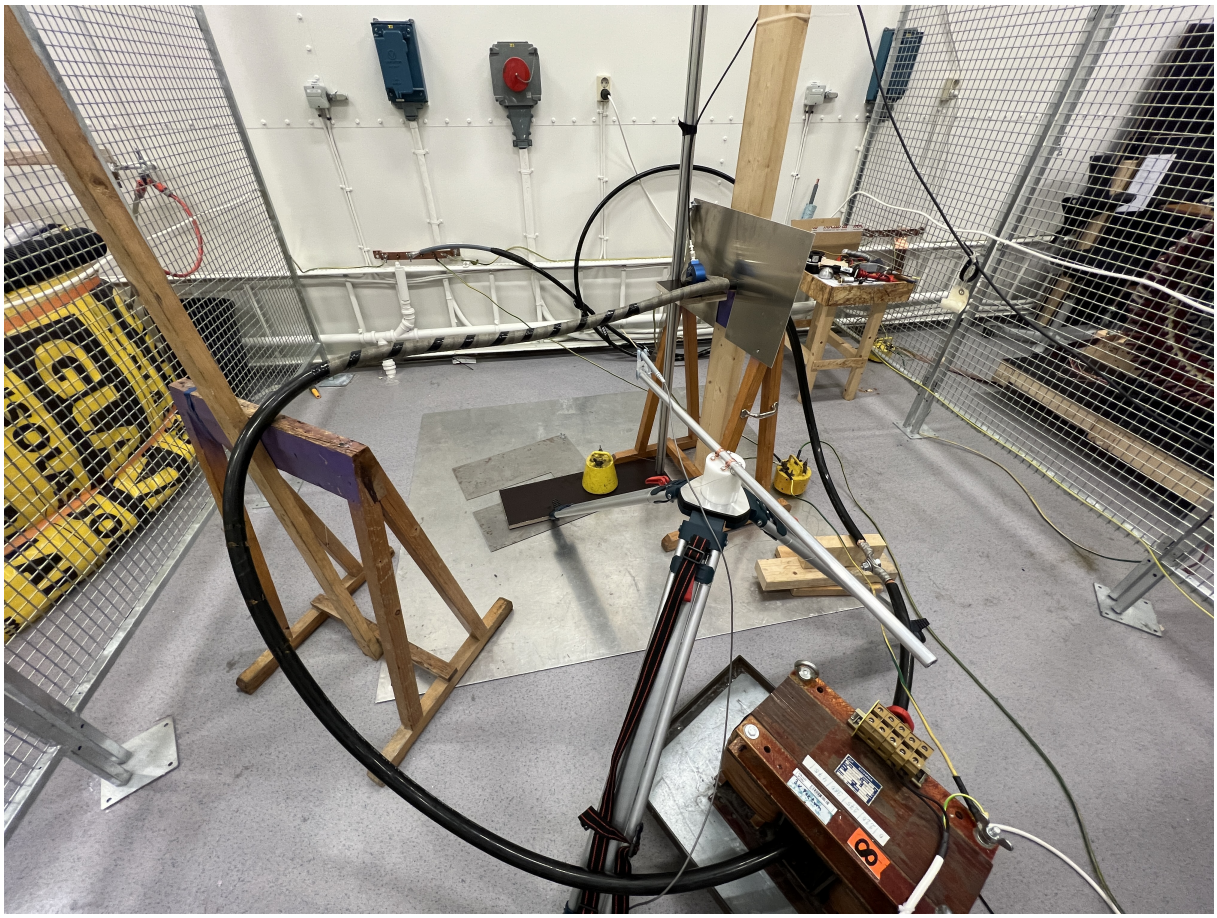

Figure A.1: Photo of the experimental setup during the 50 Hz AC current experiments.

A.2 Switching transient experiment

Table A.2: Equipment used for the test object, laboratory and measurement setup during the switching transient experiments.

Category	Equipment
Laboratory setup	Pre-setup configuration as shown in Figure 3.7
Test object	12 kV Cu PEX cable - IV termination tape - Copper mesh Tekbox TBCP1-250 HFCT - 26 dB of attenuators - Gas discharge tube
Measurement setup	FLIR C3 Thermal camera Rohde & Schwarz RTB2004 Oscilloscope Tektronix TDS2014C Oscilloscope Coaxial cable

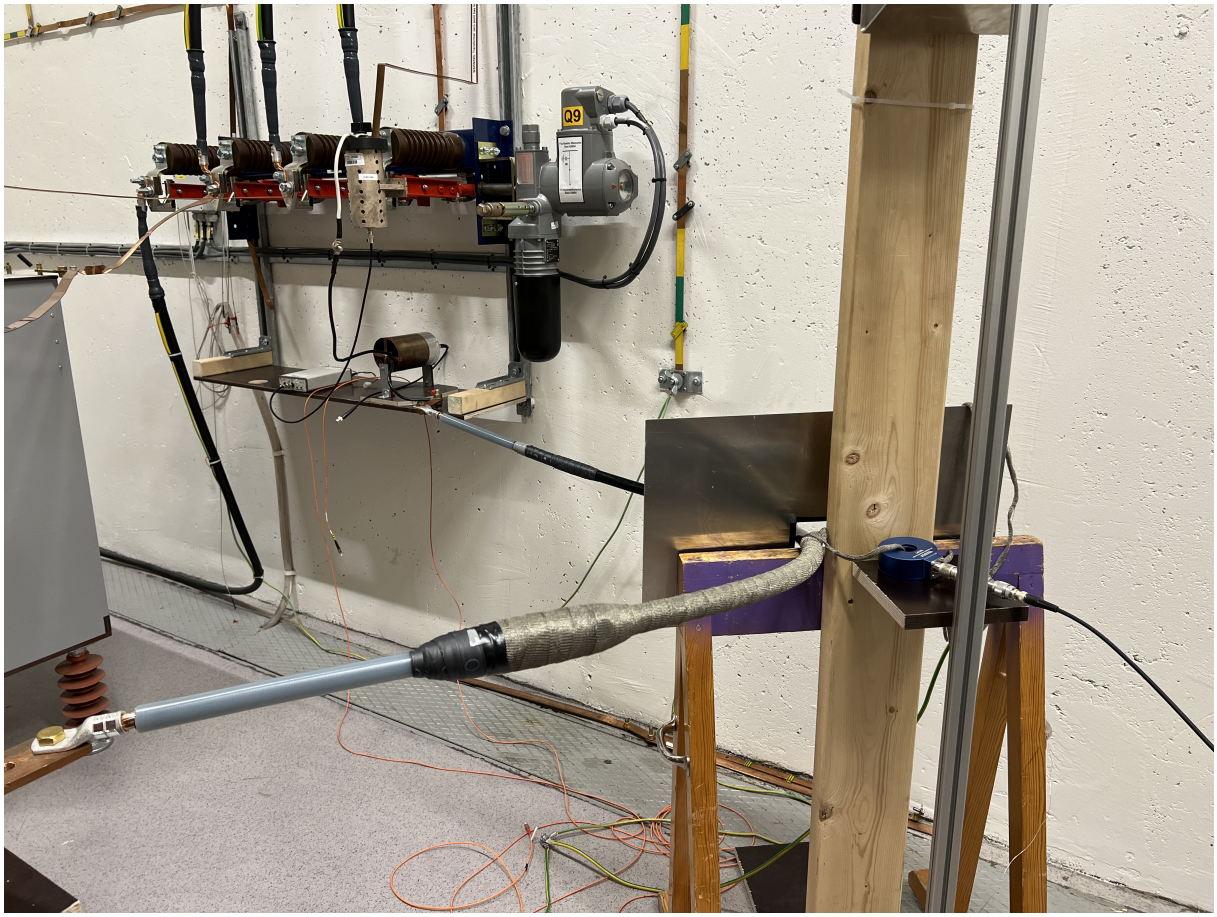

Figure A.2: Photo of the experimental setup during the switching transient experiments.

A.3 Lightning impulse experiment

Table A.3: Equipment used for the test object, laboratory and measurement setup during the lightning experiments.

Category	Equipment
Laboratory setup	High Volt - Impulse voltage test system 60/1200 515 Ω resistor Capacitive voltage divider
Test object	12 kV Cu PEX cable - IV termination tape - Copper mesh Tekbox TBCP1-250 HFCT - 20 dB of attenuators - 50 Ω termination 1:5
Measurement setup	Current probe 94606-1 - 26 dB of attenuators - 50 Ω termination 1:5 Tektronix TDS2014C Oscilloscope Coaxial cable Computer

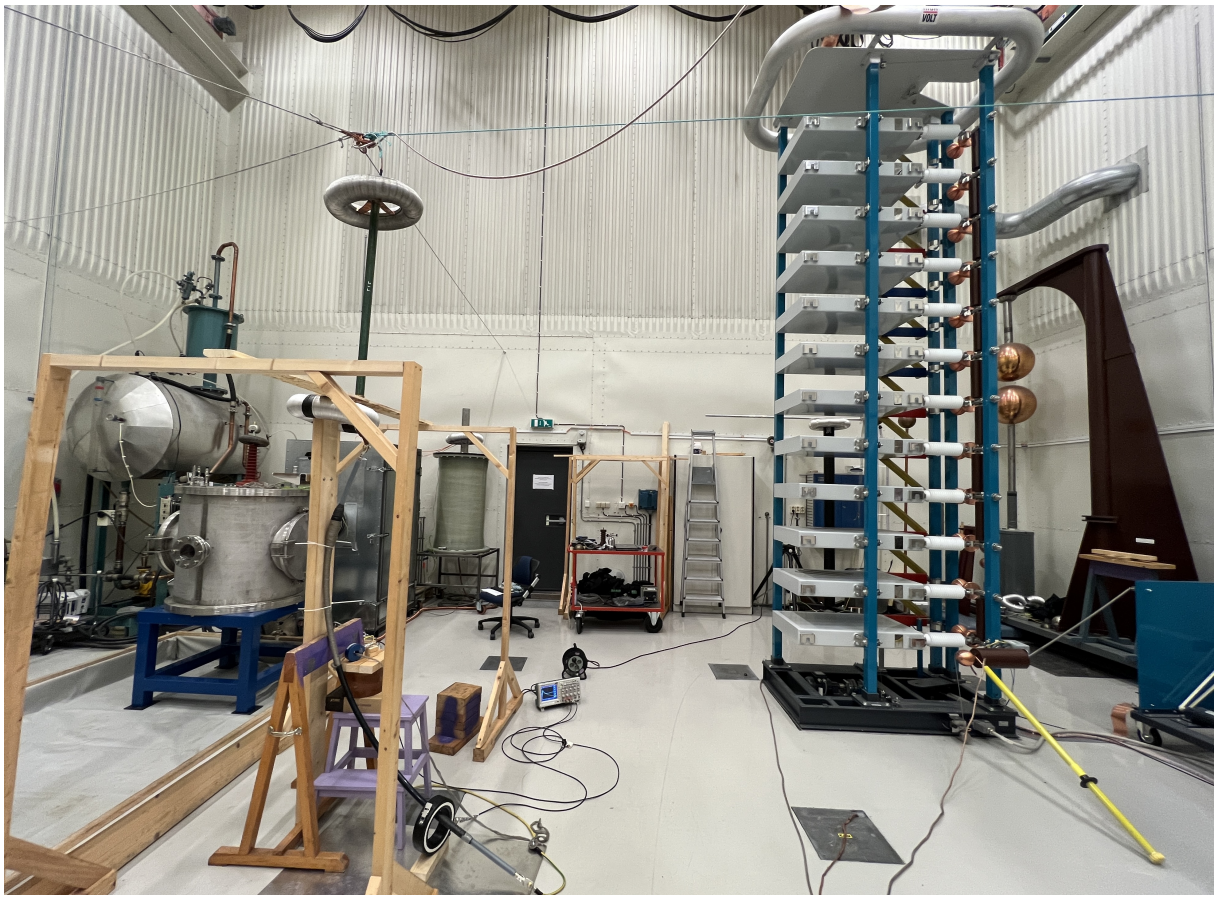

Figure A.3: Photo of the experimental setup during the lightning impulse experiments.

B Experimentally obtained HFCT output voltage

Table B.1 presents the experimentally obtained HFCT output voltage for all three HFCT orientations and at distances between 0 and 150 mm from the cable. The current was set to 1000 A for all measurements and the measurement interval was 10 mm.

Table B.1: The measured output voltages in RMS at distances from 0 to 150 mm from the cable for all three orientations.

Distance [mm]	Measured output voltage RMS [mV]		
	Orientation 1	Orientation 2	Orientation 3
0	0.466	2.357	1.999
10	0.382	1.899	1.504
20	0.326	1.546	1.229
30	0.270	1.294	0.944
40	0.216	1.087	0.779
50	0.213	0.861	0.692
60	0.208	0.691	0.559
70	0.170	0.549	0.467
80	0.170	0.457	0.400
90	0.170	0.402	0.342
100	0.170	0.343	0.309
110	0.170	0.314	0.285
120	0.170	0.285	0.230
130	0.170	0.250	0.211
140	0.170	0.226	0.191
150	0.170	0.210	0.191

C Scope images of HFCT output voltage

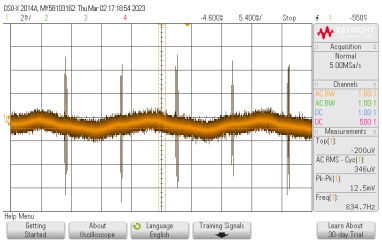
Orientation 1 - 0 mm

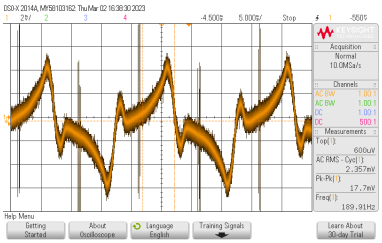
Orientation 2 - 0 mm

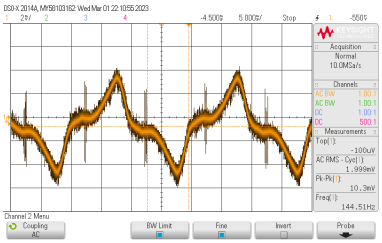
Orientation 3 - 0 mm

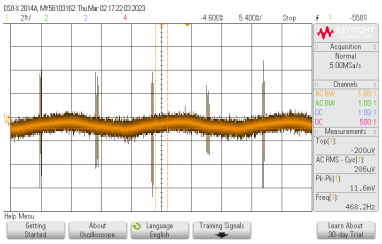
Orientation 1 - 20 mm

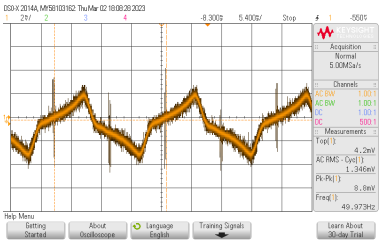
Orientation 2 - 20 mm

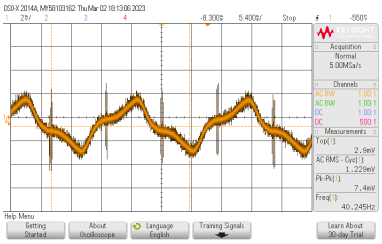
Orientation 3 - 20 mm

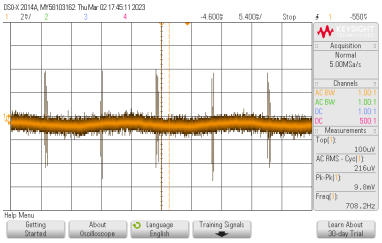
Orientation 1 - 40 mm

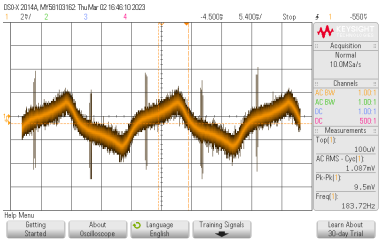
Orientation 2 - 40 mm

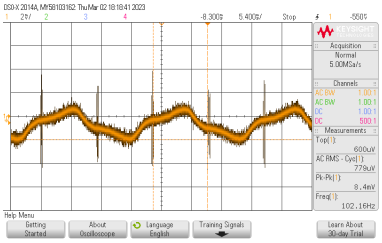
Orientation 3 - 40 mm

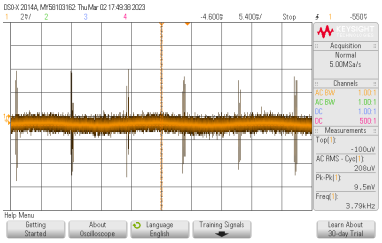
Orientation 1 - 60 mm

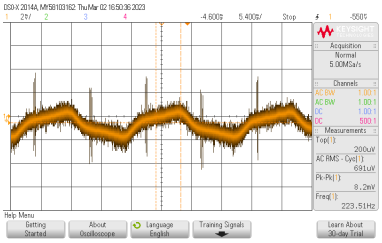
Orientation 2 - 60 mm

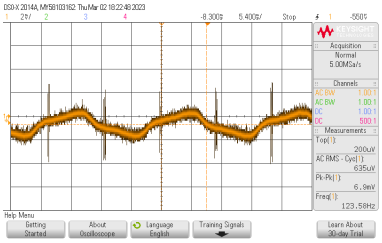
Orientation 3 - 60 mm

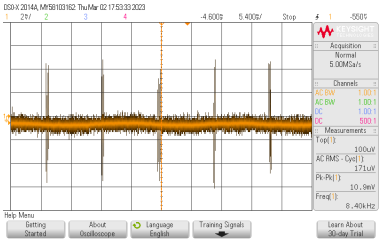
Orientation 1 - 80 mm

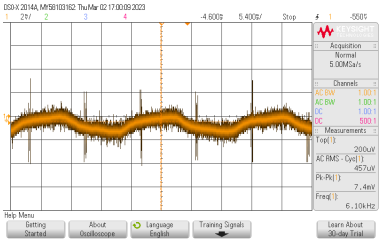
Orientation 2 - 80 mm

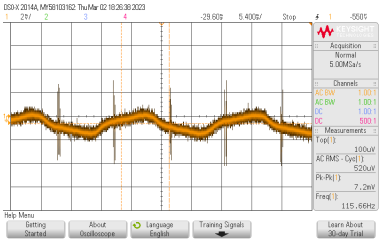
Orientation 3 - 80 mm

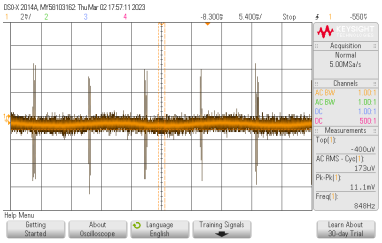
Orientation 1 - 100 mm

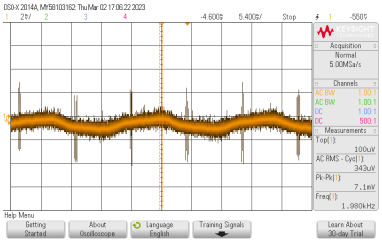
Orientation 2 - 100 mm

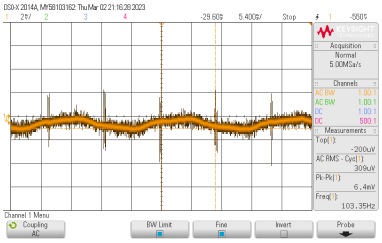
Orientation 3 - 100 mm

D Comparison of magnetic flux density

Table D.1 presents a comparison of the measured magnetic flux density between the experiments, COMSOL and analytical calculations for distances ranging from 5 to 150 mm. The current through the cable was set to 1000 A.

Table D.1: A comparison of the measured magnetic flux density at distances ranging from 5 to 150 mm. The distance is from the outer cable insulation and has a measurement interval of 5 mm.

Distance from outer	**Measured magnetic flux density [mT]**		
semi-conductor [mm]	**Experiment**	**COMSOL**	**Analytical**
5	9.38	9.98	10.00
10	7.43	7.97	8.00
15	6.28	6.68	6.67
20	5.30	5.72	5.71
25	4.55	5.00	5.00
30	4.02	4.45	4.44
35	3.58	4.00	4.00
40	3.23	3.64	3.64
45	2.91	3.34	3.33
50	2.75	3.07	3.08
55	2.63	2.86	2.86
60	2.49	2.66	2.67
65	2.31	2.51	2.50
70	2.15	2.35	2.35
75	2.04	2.22	2.22
80	1.88	2.11	2.11
85	1.77	2.00	2.00
90	1.68	1.91	1.90
95	1.61	1.82	1.82
100	1.52	1.74	1.74
105	1.42	1.67	1.67
110	1.37	1.60	1.60
115	1.31	1.54	1.54
120	1.25	1.49	1.48
125	1.18	1.43	1.43
130	1.15	1.38	1.38
135	1.08	1.33	1.33
140	1.04	1.29	1.29
145	1.01	1.25	1.25
150	0.98	1.21	1.21

E Comparison of HFCT output voltage

Table E.1 presents a comparison of the HFCT output voltage between experiment and COMSOL for orientation 1 and 2 at distances ranging from 0 to 150 mm. The current through the conductor was set to 1000 A and had a measurement interval of 10 mm.

Table E.1: A comparison of the output voltage obtained from experiment and COMSOL between 0 and 150 mm.

Distance [mm]	Orientation 1 Experiment	Orientation 1 COMSOL	Orientation 2 Experiment	Orientation 2 COMSOL
0	0.466	0.623	2.357	2.076
10	0.382	0.520	1.899	1.657
20	0.326	0.427	1.546	1.363
30	0.270	0.406	1.294	1.165
40	0.216	0.356	1.087	1.005
50	0.213	0.321	0.861	0.892
60	0.208	0.289	0.691	0.820
70	0.170	0.259	0.549	0.735
80	0.170	0.242	0.457	0.656
90	0.170	0.206	0.402	0.641
100	0.170	0.190	0.343	0.579
110	0.170	0.186	0.314	0.559
120	0.170	0.174	0.285	0.505
130	0.170	0.164	0.250	0.497
140	0.170	0.155	0.226	0.456
150	0.170	0.147	0.210	0.417

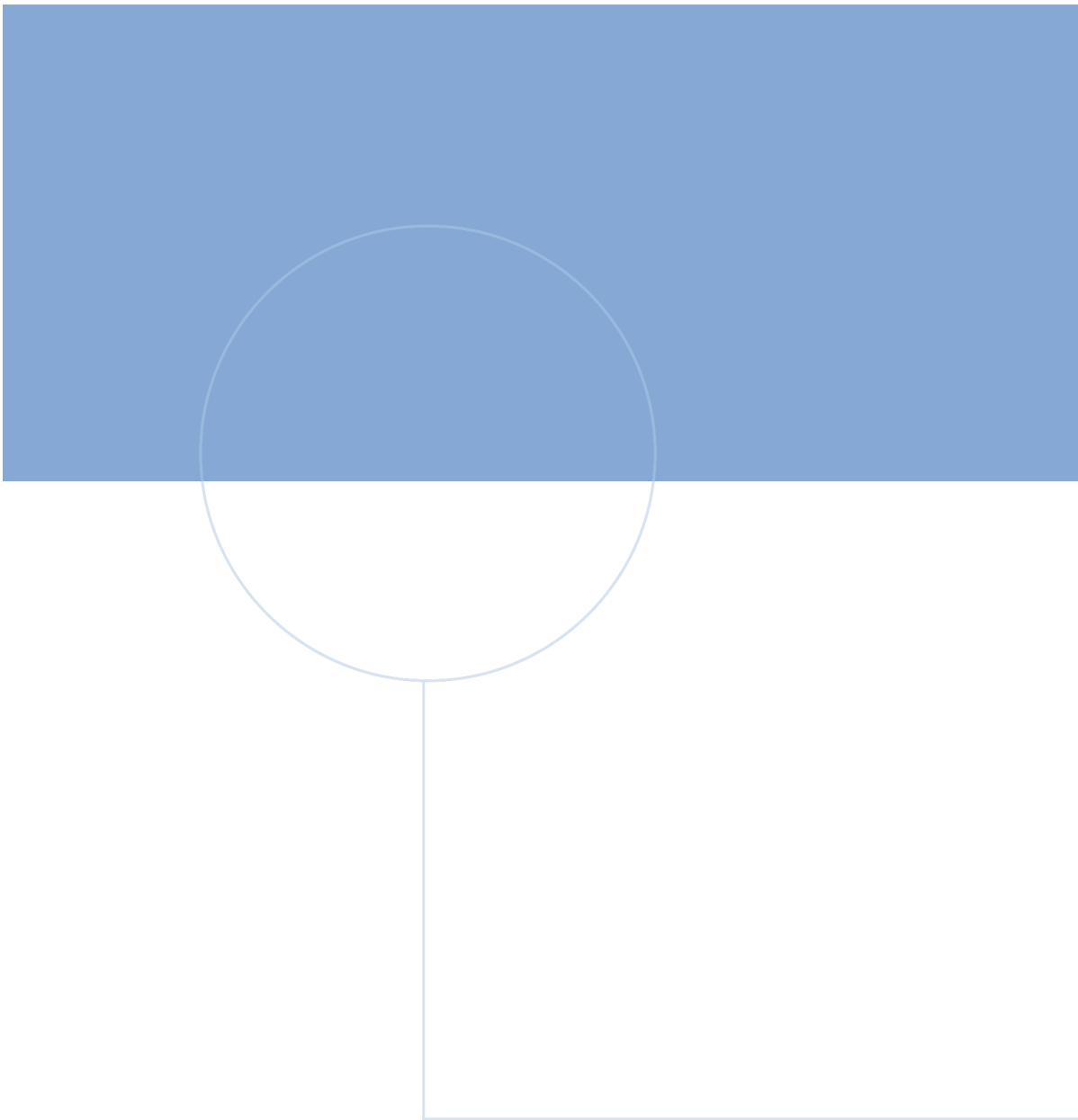

NTNU

Norwegian University of
Science and Technology